doi:10.1093/brain/awv150 BRAIN 2015: 138; 2399–2422 | 2399

BRAIN
A JOURNAL OF NEUROLOGY

Therapeutic effects of glatiramer acetate and grafted CD115$^+$ monocytes in a mouse model of Alzheimer's disease

Yosef Koronyo,[1] Brenda C. Salumbides,[1,2] Julia Sheyn,[1] Lindsey Pelissier,[1] Songlin Li,[1] Vladimir Ljubimov,[1] Michelle Moyseyev,[1] David Daley,[1] Dieu-Trang Fuchs,[1] Michael Pham,[1] Keith L. Black,[1] Altan Rentsendorj[1] and Maya Koronyo-Hamaoui[1,3]

Weekly glatiramer acetate immunization of transgenic mice modelling Alzheimer's disease resulted in retained cognition (Morris water maze test), decreased amyloid-β plaque burden, and regulation of local inflammation through a mechanism involving enhanced recruitment of monocytes. Ablation of bone marrow-derived myeloid cells exacerbated plaque pathology, whereas weekly administration of glatiramer acetate enhanced cerebral recruitment of innate immune cells, which dampened the pathology. Here, we assessed the therapeutic potential of grafted CD115$^+$ monocytes, injected once monthly into the peripheral blood of transgenic $APP_{SWE}/PS1_{\Delta E9}$ Alzheimer's disease mouse models, with and without weekly immunization of glatiramer acetate, as compared to glatiramer acetate alone. All immune-modulation treatment groups were compared with age-matched phosphate-buffered saline-injected control transgenic and untreated non-transgenic mouse groups. Two independent cohorts of mice were assessed for behavioural performance (6–8 mice/group); treatments started in 10-month-old symptomatic mice and spanned a total of 2 months. For all three treatments, our data suggest a substantial decrease in cognitive deficit as assessed by the Barnes maze test ($P < 0.0001$–0.001). Improved cognitive function was associated with synaptic preservation and reduction in cerebral amyloid-β protein levels and astrogliosis ($P < 0.001$ and $P < 0.0001$), with no apparent additive effects for the combined treatment. The peripherally grafted, green fluorescent protein-labelled and endogenous monocytes, homed to cerebral amyloid plaques and directly engulfed amyloid-β; their recruitment was further enhanced by glatiramer acetate. In glatiramer acetate-immunized mice and, moreover, in the combined treatment group, monocyte recruitment to the brain was coupled with greater elevation of the regulatory cytokine IL10 surrounding amyloid-β plaques. All treated transgenic mice had increased cerebral levels of MMP9 protein ($P < 0.05$), an enzyme capable of degrading amyloid-β, which was highly expressed by the infiltrating monocytes. *In vitro* studies using primary cultures of bone marrow monocyte-derived macrophages, demonstrated that glatiramer acetate enhanced the ability of macrophages to phagocytose preformed fibrillar amyloid-β_{1-42} ($P < 0.0001$). These glatiramer acetate-treated macrophages exhibited increased expression of the scavenger receptors CD36 and SCARA1 (encoded by *MSR1*), which can facilitate amyloid-β phagocytosis, and the amyloid-β-degrading enzyme MMP9 ($P < 0.0001$–0.001). Overall, our studies indicate that increased cerebral infiltration of monocytes, either by enrichment of their levels in the circulation or by weekly immunization with glatiramer acetate, resulted in substantial attenuation of disease progression in murine Alzheimer's models by mechanisms that involved enhanced cellular uptake and enzymatic degradation of toxic amyloid-β as well as regulation of brain inflammation.

1 Department of Neurosurgery, Maxine-Dunitz Neurosurgical Institute, Cedars-Sinai Medical Centre, Los Angeles, CA 90048, USA
2 F. Widjaja Foundation Inflammatory Bowel and Immunobiology Research Institute, Cedars-Sinai Medical Centre, Los Angeles, CA 90048, USA
3 Department of Biomedical Sciences, Cedars-Sinai Medical Centre, Los Angeles, CA 90048, USA

Received October 20, 2014. Revised March 6, 2015. Accepted April 7, 2015. Advance Access publication June 6, 2015

Correspondence to: Maya Koronyo-Hamaoui,
Departments of Neurosurgery and Biomedical Sciences,
Cedars-Sinai Medical Center,
Los Angeles, CA 90048, USA
E-mail: koronyom@cshs.org

Keywords: Alzheimer's disease; neuroprotection; ; neuroinflammation; ; dementia; ; behavioural neurology

Abbreviations: ADtg = Alzheimer's disease double transgenic $APP_{SWE}/PS1_{\Delta E9}$; BM = bone marrow; GA = glatiramer acetate; GFP = green fluorescent protein; Mo^{BM} = bone marrow-derived $CD115^+$ monocytes; $M\Phi^{BM}$ = monocyte-derived macrophages

Introduction

Alzheimer's disease is tightly linked to the cerebral accumulation of amyloid-β protein, particularly neurotoxic soluble amyloid-$\beta_{1–42}$ peptides and extracellular aggregations of amyloid-β plaques (Hardy and Selkoe, 2002; Selkoe, 2008; Shankar *et al.*, 2008; Rimoldi *et al.*, 2010). The substantial increase in amyloidogenic amyloid-β forms is associated with neuroinflammation and downstream intracellular neurofibrillary tangles containing abnormal tau protein (encoded by *MAPT*). These are believed to be key contributors to synaptic and neuron loss leading to cognitive decline (Akiyama *et al.*, 2000*b*; Bales *et al.*, 2000; McGeer and McGeer, 2002; Wyss-Coray and Mucke, 2002; Selkoe, 2008).

Age-dependent accumulation of cerebral amyloid-β in sporadic forms of Alzheimer's disease appears to be due to insufficient clearance of amyloid-$\beta_{1–42}$ (Saido, 1998; Mawuenyega *et al.*, 2010) rather than its overproduction, as observed in cases with familial Alzheimer's disease (Potter *et al.*, 2013). The clearance of amyloidogenic amyloid-β forms is regulated by multiple mechanisms including removal by innate immune cells (Wyss-Coray *et al.*, 2001; Simard *et al.*, 2006; Takata *et al.*, 2007; Richard *et al.*, 2008; Bates *et al.*, 2009; Lai and McLaurin, 2012). Growing evidence supports the concept that activated inflammatory cells, brain-residing microglia, and, moreover, infiltrating monocyte-derived macrophages are critical for the physiological clearance of amyloid-β (Malm *et al.*, 2005; Simard *et al.*, 2006; Butovsky *et al.*, 2007; El Khoury *et al.*, 2007; Koronyo-Hamaoui *et al.*, 2009). Phagocytosis and enzymatic degradation are key functions by which myelomonocytes may enhance amyloid-β clearance (Frautschy *et al.*, 1992; Paresce *et al.*, 1996; Fiala *et al.*, 2005; Majumdar *et al.*, 2008; Lebson *et al.*, 2010; Bernstein *et al.*, 2014). However, although resident microglia under chronic inflammatory conditions (i.e. Alzheimer's disease) become highly pro-inflammatory, inefficient in removing amyloid-β, and eventually cytotoxic to neurons, blood-borne recruited macrophages exhibit an increased phagocytic ability to remove amyloid-β plaque (Simard *et al.*, 2006; Butovsky *et al.*, 2007; Koronyo-Hamaoui *et al.*, 2009; Lai and McLaurin, 2012; Malm *et al.*, 2012). The phagocytic abilities of macrophage to clear amyloid-β were associated with expression of specific cell surface receptors such as the class B scavenger receptor CD36 and the class A type 1 scavenger receptor SCARA1 (encoded by *MSR1*), which bind ligands including amyloid-β and facilitate their cellular uptake (Hickman *et al.*, 2008; Yamanaka *et al.*, 2012; Frenkel *et al.*, 2013). Moreover, macrophages may confer further neuroprotection in Alzheimer's disease via regulation of harmful inflammation and delivery of mediators of neural repair and regeneration (Butovsky *et al.*, 2006; Wyss-Coray, 2006; Glezer *et al.*, 2007; Koronyo-Hamaoui *et al.*, 2009; Malm *et al.*, 2010; Bakalash *et al.*, 2011).

Immune modulation achieved by immunization with weak agonists of myelin-derived antigens, glatiramer acetate (GA), or altered MOG-derived peptide, which are known to induce peripheral and brain T cell responses, substantially limited the pathology and behavioural deficits associated with Alzheimer's disease in double-transgenic $APP_{SWE}/PS1_{\Delta E9}$ mice (Frenkel *et al.*, 2005; Butovsky *et al.*, 2006; Koronyo-Hamaoui *et al.*, 2009; Bakalash *et al.*, 2011; Koronyo-Hamaoui *et al.*, 2011). Both types of immunizations led to increased cerebral infiltration of monocyte-derived macrophages associated with a shift toward an anti-inflammatory profile of lower TNFα (encoded by *TNF*) and higher IL10, TGF-β1 (encoded by *TGFB1*), and the neurotrophic factor IGF1 (Butovsky *et al.*, 2007; Koronyo-Hamaoui *et al.*, 2009). Peripheral ablation of bone marrow-derived $CD11c^+$ myeloid cells or inhibition of their recruitment to the brain exacerbated disease progression (Butovsky *et al.*, 2007; El Khoury *et al.*, 2007).

In the present study we investigated the therapeutic potential and the cellular, synaptic and molecular changes following GA immunization, bone marrow-derived $CD115^+$ monocyte subset blood enrichment, and the combined treatment of GA and monocyte enrichment in murine models of Alzheimer's disease. The data indicate that in symptomatic $APP_{SWE}/PS1_{\Delta E9}$ (ADtg) mice, these three types of immune-modulation treatments led to a substantial diminution of cognitive deficits and Alzheimer's disease-related neuropathology coupled with increased synaptic preservation and spontaneous recruitment of blood-grafted monocytes to amyloid-β plaques. The results of the *in vitro* studies indicated that GA directly increased the ability of macrophage to clear amyloid-$\beta_{1–42}$ fibrils via mechanisms

involving increased class A and B scavenger receptors and amyloid-β-degrading enzyme expression.

Materials and methods

Mice

Alzheimer's disease double transgenic $APP_{K595N,\ M596L}$ + $PS1_{\Delta E9}$ (ADtg) mice from the B6.Cg-Tg (APPswe, PSEN1ΔE9) 85Dbo/J strain and their age-matched non-transgenic (wild-type) littermates were purchased from Jackson Laboratories (Stock #005864) and then bred and maintained at Cedars-Sinai Medical Centre. These ADtg mice carry the human transgene, which allows detection of amyloid-β forms using anti-human antibodies. All mice in this study have a C57BL/6 congenic background. Two cohorts of mice (all male) were used for behavioural, histological, and biochemical analysis. An additional ADtg mouse cohort (equal numbers male and female) was used to evaluate innate immune infiltration to the brain by flow cytometry. For *in vitro* studies, primary cell cultures, and characterization of isolated CD115+ monocytes before and after magnetic-activated cell sorting (MACS) column selection, the bone marrow donor mice were young non-transgenic wild-type littermates (8–10 weeks of age). For adoptive transfer of bone marrow-derived monocytes, the donor mice were young (8–10 weeks of age) C57BL/6-transgenic (UBC-GFP) 30 Scha/J mice expressing enhanced green fluorescent protein (GFP) under the direction of the human ubiquitin C promoter (Stock #004353). For flow cytometry studies assessing monocyte infiltration into ADtg brains, the donors were young non-transgenic wild-type mice (8–10 weeks of age). All experiments were conducted according to regulations of the Cedars-Sinai Medical Centre Institutional Animal Care and Use Committee (IACUC) under an approved protocol. In addition, all experiments were conducted and recorded by researchers blinded to the mouse genotypes.

Genotyping

Genomic DNA was extracted from the tip of the mouse tail by using a DNA extraction kit (Qiagen) and following the manufacturer's protocol. Double-transgenic $APP_{SWE}/PS1_{\Delta E9}$ mice and non-transgenic wild-type littermates were identified by genotyping for the presence of the transgenes by PCR, as previously described (Jankowsky *et al.*, 2001, 2004; Butovsky *et al.*, 2006).

Glatiramer acetate immunization

ADtg mice (10 months old) received subcutaneous injections of GA [also known as Cop-1 and Copaxone®; 100 µg in phosphate-buffered saline (PBS)] or PBS alone (control group) twice a week for 1 week and then once a week for 8 weeks. For evaluation of innate immune infiltration to the brain by flow cytometry, 10-month-old ADtg mice received subcutaneous injections of GA (100 µg in PBS) or PBS alone twice a week for 1 week and then once a week for 3 weeks. At the end of the study, all mice were anaesthetized and then perfused with ice-cold PBS, after which their organs were collected and analysed or fixed in 2.5% paraformaldehyde (Sigma-Aldrich) following dehydration with 30% sucrose for further histological analysis.

Isolation and adoptive transfer of bone marrow-derived CD115+ monocytes

CD115+ monocytes from mice donors were isolated as previously reported (Varol *et al.*, 2007; Shechter *et al.*, 2009). In brief, bone marrow cells were harvested from the femora, tibiae, and humeri and enriched for mononuclear cells on a Ficoll-Paque® PLUS (17-1440-03, GE Healthcare) density gradient. The CD115+ monocyte population was isolated through MACS enrichment column using the biotinylated anti-CD115 mAb clone AFS98 (#13-1152; eBioscience) and streptavidin-coupled magnetic beads (Miltenyi Biotec), according to the manufacturer's protocols. After this procedure, monocytes ($5–6 \times 10^6$ cells/mouse) were injected into the tail veins of 10-month-old ADtg mice once a month for 2 months (see the experimental procedure in Fig. 1). For evaluation of innate immune infiltration to the brain by flow cytometry, 10-month-old ADtg mice received one injection of bone marrow-derived CD115+ monocytes (same dose as above).

Flow cytometry and immunohistochemical characterization of bone marrow-derived CD115+ monocytes

Bone marrow cells were harvested from young donor wild-type mice ($n = 3–4$ mice per experiment) as detailed above. After enrichment for mononuclear cells by Ficoll® gradient, one portion of cells was collected (before CD115+ column), and a second portion of cells underwent further isolation for CD115+ monocyte population (after CD115+ column), using the MACS enrichment column as detailed above. Both cell portions, before and after CD115+ column, were either immediately stained and analysed by flow cytometry or plated to generate macrophage cultures for further immunohistochemical analysis (see Supplementary Fig. 4). For flow cytometry analysis, the before CD115+ column cells were stained with the following antibodies: biotinylated anti-CD115 mAb clone AFS98 (#13-1152; eBioscience), APC-conjugated anti-Biotin clone Bio3-18E7 (#130-090-856; Miltenyi Biotec), PE-conjugated anti-CD36 clone REA262 (#130-102-763; Miltenyi Biotec), Viobright FITC-conjugated anti-CD36 clone REA262 (#130-104-889; Miltenyi Biotec), PE-conjugated anti-CD204 clone REA148 (#130-102-328; Miltenyi Biotec), and Alexa Fluor® 488-conjugated anti-MMP9 polyclonal antibody (#bs-0397R-A488; Bioss). For the after CD115+ column cells, we used a set of staining antibodies identical to that specified above but excluded the primary anti-CD115 mAb because this isolation procedure already linked the biotinylated anti-CD115 antibody to the cells. All antibody dilutions were 1:100. The labelled samples were analysed on a BD LSRFortessa™ Cell Analyzer equipped with BD FACS Diva software; data were further analysed with FlowJo software (vX.0.7r2; Tree Star, Inc.).

Both cell portions, before and after CD115+ column selection, were also differentiated into primary macrophage cultures and analysed by immunohistochemistry. In brief, cells were differentiated into macrophages by 7-day cultivation in complete RPMI-1640 medium (#21870; Life Technologies) with 10% serum and 20 ng/ml MCSF

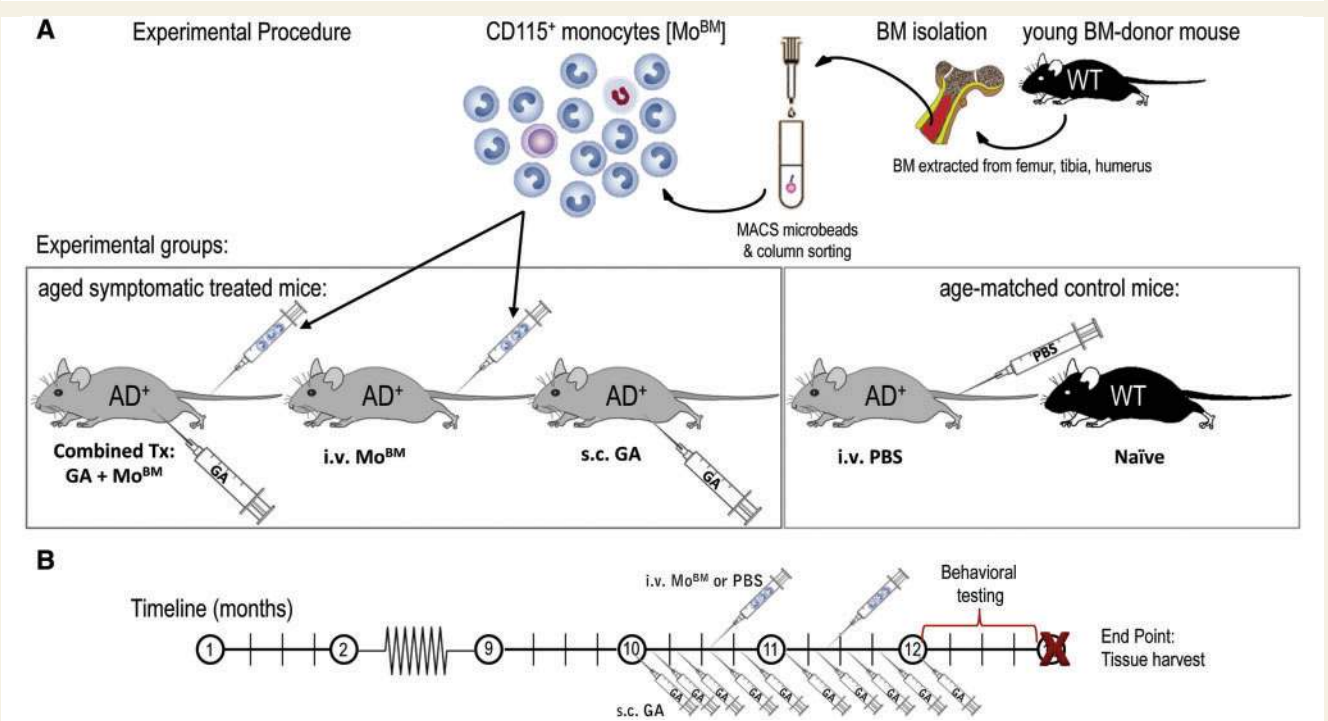

Figure 1 Scheme of the experimental procedure and immunization timeline. (**A**) Experimental procedure demonstrating the adoptive transfer of monocytes to the peripheral blood of ADtg mice. CD115$^+$ monocytes (Mo^{BM}) were isolated from the bone marrow of young (8- to 10-week-old) wild-type mice and enriched (~95%, see Supplementary Fig. 4A) by MACS microbeads and an anti-CD115 antibody column sorting procedure. Mo^{BM} were then intravenously (i.v.) injected into the tail vein of older (10-month-old) ADtg mice. Additional experimental groups included ADtg mice that were subcutaneously (s.c.) immunized with GA or received combined GA and Mo^{BM} treatment. Age- and sex-matched controls are also indicated. (**B**) Experimental timeline. At 10 months of age, mice received immunization regimens of either weekly injections of GA and/or monthly injections of Mo^{BM} or PBS over a 2-month period. After completion of the treatment period, the mice (now 12 months old) underwent behavioural testing (Barnes maze hippocampus-dependent learning and memory test). The brain tissues at 13 months were harvested for subsequent analysis. BM = bone marrow; AD + = ADtg; WT = wild-type.

(#315-02; PeproTech). Primary cultures of macrophage were then plated at 1.2×10^5 cells per well (3–4 wells for each condition) in 24-well tissue-culture plates on glass coverslips overnight. Methanol (99.8%) at −20°C for 20 min was used for fixation of the cells followed by repeated washes with PBS. Cells were then stained using rat anti-CD36 mAb clone MF3 (1:200; ab80080; Abcam), rat anti-CD204 scavenger receptor type I/II (SCARA1) mAb (1:100; MCA1322; AbD Serotec), and goat anti-MMP9 pAb (1:100; AF909; R&D systems). Secondary polyclonal antibodies included donkey anti-rat and anti-goat conjugated with Cy2, Cy3 or Cy5 (1:200; Jackson ImmunoResearch Laboratories). The cells were mounted using ProLong® Gold with DAPI (Molecular Probes, Life Technologies). Several fields (minimum $n = 4$ randomly selected per group) were obtained from each well using a Carl Zeiss Axio Imager Z1 Apotome-equipped microscope (an average of 120 cells in each field). Images were obtained using the same exposure time in each occasion. The fluorescent signal and its total area were determined and quantified by the conversion of the individual images to grey scale and standardizing to baseline using histogram-based thresholds with NIH ImageJ software. The 'area/cell' measures the total fluorescent signal (area) divided by the total number of cells (DAPI count) of the same field (image). For all experiments, the investigators were blinded to the treatment condition.

Barnes maze behavioural test in mice

The Barnes maze is a spatial-learning task that allows subjects to use spatial cues to locate a means of escape from a mildly aversive environment (open space with light projection); mice are required to use spatial cues to find an escape location. The mice are assessed for their ability to learn the location of an escape box over the course of 9 days in the Barnes maze apparatus. This timing was established based on significant differences between wild-type and PBS groups, and was found suitable to test the effects of our treatments. The Barnes maze apparatus is a circular table in which 20 holes are located equidistantly around the perimeter. During a trial the escape box is placed under one of these holes, whereas false boxes, too small to be entered, are placed beneath the other 19 holes. The animals are first placed into an opaque cylinder at the centre of the maze for 30 s to promote initial spatial disorientation. After this time, the cylinder is removed and the animal explores the maze until it finds and enters the escape box, leading to its return to the home cage. The escape latency is the duration of time between removal of the cylinder and the animal's entry into the escape box. The errors (incorrect entries) represent the number of events in which the mouse enters a false box. Two bright lights illuminate the centre of the Barnes

platform. If the mouse fails to enter the escape box within 5 min (300 s), the experimenter leads it to the escape box. The animal remains in the escape box for an additional 30 s before it is removed and taken to the home cage. All boxes and the maze surface are sprayed with 70% isopropyl alcohol and wiped in a non-systematic fashion to dissipate odour cues for the subsequent trial. The location of the escape box remains the same during every trial of the training/acquisition phase and is shifted between mice to reduce the potential for unintended intra-maze cues. Training is repeated three times per day with a 15-min interval separating each trial. Data from each trial are retained and averaged. The training/acquisition phase is 4 days. Following this is a 2-day break without any exposure to the maze. On Day 7, each animal is retested during a three-trial session by using the same escape box location and method from the training/acquisition phase. On Day 8, following the memory retention phase, the reversal phase begins. The escape box is placed in a quadrant different from the original escape box location. Using the same procedure detailed above, reversal trials are repeated three times per day over two consecutive days (Days 8 and 9). The second cohort of mice underwent the same Barnes maze test, except that each session time was shortened to a maximum of 4 min (240 s), as this length of time was shown to be as effective as the longer period (5 min). All investigators were blinded to the mouse groups. Data were recorded manually, digitally, and by a video camera located above the maze.

Immunohistochemistry

Brain coronal cryosections (30-µm thick) were treated with a permeabilization and blocking solution containing 20% normal horse serum (Invitrogen) and 0.05% Triton™ X-100 (Sigma-Aldrich). Sections were stained overnight at 4°C with combinations of the following primary antibodies [either monoclonal (mAb) or polyclonal (pAb)] in 2% blocking solution in PBS: mouse anti-human amyloid-β [residues 17–24, mAb clone 4G8 (1:100; SIG-39220; Covance) and residues 1–16, mAb clone 6E10 (1:100; SIG-39320; Covance)], rabbit anti-GFAP pAb (1:100; G926; Sigma-Aldrich), rabbit anti-Iba1 pAb (1:250; #019-19741; Wako Chemicals), rabbit anti-GFP pAb (1:500; #598; MBL), rat anti-CD45 mAb clone 30-F11 (1:25; #550539; BD Pharmingen), goat anti-IL10 pAb (1:100; AF519; R&D systems), and goat anti-MMP9 pAb (1:100; AF909; R&D systems). Secondary polyclonal Abs (donkey anti-mouse, anti-rat, anti-goat, and anti-rabbit; 1:200; Jackson ImmunoResearch Laboratories) conjugated with Cy2, Cy3, Cy5, or DyLight™ 649, were incubated for 1 h at 37°C. The sections were washed in PBS and mounted using Vectashield (Vector Laboratories) containing 4',6-diamidino-2-phenylindole dihydrochloride (DAPI) (H-1200) or not containing DAPI (H-1000), or ProLong® Gold with DAPI (Molecular Probes, Life Technologies). Negative controls were processed using the same protocol with the omission of the primary antibody to assess non-specific labelling. For microscopic analysis, we used a Carl Zeiss Axio Imager Z1 fluorescence microscope equipped with ApoTome (Carl Zeiss MicroImaging, Inc.). For processing and analysis of the images, we used AxioVision (release 4.6.3) software (Carl Zeiss).

Presynaptic labelling and quantification of synaptic area in the hippocampus

To define the synaptic area in the hippocampus of ADtg and non-transgenic (wild-type) mice, three independent coronal brain sections at bregma −2.50, −2.65, and −2.80 mm (Liang *et al.*, 2011) per animal ($n = 6$ mice per group) were stained with the presynaptic marker VGluT1 (encoded by *Slc17a7*) (Chemicon, guinea pig, 1:6000). For each hippocampal field, high-resolution scans were acquired using × 100 oil objective lens and the Zeiss ApoTom mode. Optical sectioning included 15 *Z*-stack images, each 0.25-µm wide and covering focal planes within a tissue depth of 3.75 µm. Sections from all five groups, obtained at the same level, were identically immunostained. During all experiments, no-primary and no-secondary antibody controls were run in parallel. There was no specific staining with these controls. To cover the hippocampal area, 15 rectangle fields (each 90 µm × 70 µm) were precisely selected in the lateral and medial blade molecular layer of the dentate gyrus, as well as in the stratum lacunosum-moleculare, stratum radiatum, and stratum oriens of the cornu ammonis 1 (CA1), as illustrated in Fig. 3F. The parameters for scanning remained the same across treatment conditions. Single optical section images were analysed using the NIH ImageJ macro and batch process to quantify the synaptic area (15 optical sections/field, 15 fields/brain section, and 675 total images/brain). The average synaptic area or percentage of the area per image was calculated for each condition.

Thioflavin-S amyloid-β plaque staining

Following secondary antibody staining, the brain sections were stained with thioflavin-S (Thio-S, 1% w/v in 70% ethanol) (Sigma-Aldrich) for 10 min at room temperature, washed three times in 70% ethanol, and then washed once in distilled water, for 1 min each.

Quantification and stereological counting procedure

The number and area (µm^2) of Thio-S$^+$ and 4G8$^+$ amyloid-β plaques as well as those of GFAP$^+$ and Iba1$^+$CD45^{hi} cells were determined by examining four to six coronal sections per mouse at 150-µm intervals over an area covering both the hippocampal and cortical (including entorhinal and cingulate cortex) regions. For Iba1$^+$/CD45^{hi} quantification we selected only Iba1$^+$ cells labelled intensely with CD45 antibody, while excluding Iba1$^-$ cells. The CD45$^+$ cells (out of Iba1$^+$ cells) were converted into greyscale images and a threshold for intense/high signal was determined in ImageJ software once and applied to all images for CD45^{high} quantification. The fluorescence of specific signals was captured using the same exposure time for each image. Images were converted to greyscale and standardized to baseline using histogram-based thresholds with NIH ImageJ software (versions 1.38x and 1.46r). In addition, manual counting of amyloid-β plaques as well as GFAP$^+$ and Iba1$^+$/CD45^{hi} cells was done with the aid

of ImageJ software using the 'analyze' grid. Analysers who were blinded to the mouse groups performed all counts.

Flow cytometry analysis of cerebral monocyte infiltration

Experimental ADtg mice ($n = 4$–6 mice/group) were perfused with cold saline supplemented with 0.5 µM EDTA (pH8.0, Invitrogen) before harvest. Whole brains were then mechanically minced in a 70-µm cell strainer (Falcon; Corning Inc.) with ice-cold 2% foetal bovine serum (Atlanta Biological) in PBS. After centrifugation, homogenization and washing, the pellet was suspended in 40% sterile Percoll (GE Healthcare) and centrifuged for 25 min at 850*g*. The cell pellet was resuspended in 70% Percoll and centrifuged for another 20 min at 800*g*. Cells located in the top layer after the Percoll gradient were collected and washed. Next, cells were stained with the following antibodies purchased from Biolegend: FITC-conjugated anti-CD11b clone M1/70 (1:100, #101206); PE-conjugated anti–Ly-6C clone HK1.4 (1:100, #128007); and PE/Cy7-conjugated anti–CD45.2 clone 104 (1:100, #109830). The stained samples were analysed on a BD LSRFortessa Cell Analyzer equipped with BD FACS Diva software, and data were further analysed with FlowJo software (vX.0.7r2; Tree Star, Inc.).

Biochemical determination of amyloid-$\beta_{1\text{-}40}$, amyloid-$\beta_{1\text{–}42}$, MCP1, IL10 and MMP9 levels by sandwich ELISA

For brain soluble and insoluble ELISA analyses, brain tissues were thoroughly homogenized (Argos homogenizer) in PBS buffer with 0.5% Triton™ X-100 (T8787; Sigma) and protease inhibitor cocktail set I (#539131; Calbiochem). After removal of cell debris, the homogenate was centrifuged at 10 000*g* for 25 min at 4°C. The supernatant was considered the 'soluble' fraction and was used to assess soluble amyloid-$\beta_{1\text{–}40}$, amyloid-$\beta_{1\text{–}42}$, MCP1 (encoded by *Ccl2*), IL10, and MMP9 levels. The pellet was then diluted and homogenized with the above homogenizing buffer. This was the 'insoluble' fraction and was used to assess insoluble amyloid-$\beta_{1\text{–}40}$ and amyloid-$\beta_{1\text{–}42}$. After determination of protein concentration using the Pierce BCA Protein Assay Kit (#23227; Thermo Scientific), soluble and insoluble transgenic-derived amyloid-$\beta_{1\text{–}42}$ and amyloid-$\beta_{1\text{–}40}$ levels were determined. For this analysis, an anti-human amyloid-$\beta_{1\text{-}42}$ end-specific sandwich ELISA kit (KHB3442, Invitrogen; which does not recognize mouse amyloid-β nor human amyloid-β_{40}/amyloid-β_{43}) and an anti-human amyloid-$\beta_{1\text{-}40}$ end-specific sandwich ELISA kit (KHB3482, Invitrogen; which does not recognize mouse amyloid-β nor human amyloid-β_{42}/amyloid-β_{43}), were used according to the manufacturer's instructions. These kits use a combination of two antibodies specific for the N- and the COOH-termini of amyloid-$\beta_{1\text{-}42}$ or amyloid-$\beta_{1\text{-}40}$ sequences. The bound rabbit anti-COOH-terminus was detected through the use of a horseradish peroxidase-labelled anti-rabbit antibody and was read at 450 nm using a microplate reader (Spectra Max 384 plus, Molecular Devices). Soluble MCP1, IL10, and MMP9 levels were measured using the mouse/rat CCL2/JE/MCP1 Quantikine® ELISA Kit (MJE00), Mouse IL10 Quantikine® ELISA Kit (M1000B), and Mouse Total MMP-9 Quantikine® ELISA Kit (MMPT90), respectively, all according to the manufacturer's instructions (R&D systems). The optical density of each well was read at 450 nm (with 540 nm correction) using the same microplate reader.

Preparation of amyloid-$\beta_{1\text{–}42}$ fibrils

Lyophilized non-fluoro amyloid-$\beta_{1\text{–}42}$ peptide (#20276; Anaspec) was initially monomerized by dissolving it in ice-cold HFIP (hexafluoroisopropanol) (#52512; Sigma) to a final concentration of 1 mM and then aliquoted in sterile siliconized microcentrifuge tubes. The HFIP was first evaporated while in the sterile hood and then under vacuum conditions in a SpeedVac for 2 h to remove any trace of HFIP; the peptide film was stored at −20°C until use. To induce fibril formation, fluoro (HiLyte647; #64161; Anaspec) and non-fluoro amyloid-$\beta_{1\text{–}42}$ films were resuspended in media to which 10% of sterile NaOH 60 mM was first added and the media were vortexed for 30 s. Then, a sterile 45% H_2O and a sterile 45% solution of 20 mM $NaH_2PO_4 + Na_2HPO_4$ (pH 7.4) were added, and the media were vortexed again and incubated on a shaker for 2 weeks at 37°C. Pre-formed amyloid-$\beta_{1\text{–}42}$ fibrils were then sonicated for 60 s and diluted to 100 nM using the same media prior to the phagocytosis assay.

Primary cultures of bone marrow-derived macrophage and the phagocytosis assay

To test amyloid-β phagocytosis by macrophage, in repeated experiments monocytes were isolated from the bone marrow of wild-type mice ($n = 18$ mice) and differentiated into macrophage by 7-day cultivation in complete RPMI-1640 medium (#21870; Life Technologies) with 10% serum and 20 ng/ml MCSF (#315-02; PeproTech). Primary cultures of macrophage were then plated at 1.2×10^5 cells per well (3–4 wells for each condition) in 24-well tissue-culture plates on glass coverslips overnight. Next, macrophages were either treated with 30 µg/ml GA (Copaxone®; TEVA Neuroscience) for the duration of 1, 3, or 24 h, or not treated (control group). Before addition of fibrillar amyloid-$\beta_{1\text{–}42}$, the cells were chilled in a 4°C ice bath for 5 min; immediately after addition of the preformed fibrillar amyloid-$\beta_{1\text{–}42}$ (100 nM), the plates were centrifuged at 515g in 25°C followed by incubation at 37°C for 30 or 60 min. The cells were then rinsed with amyloid-β-free medium to remove non-incorporated amyloid-β and later washed twice with PBS. Methanol (99.8%) at −20°C for 20 min or 4% paraformaldehyde at room temperature for 12 min was used for fixation of the cells followed by repeated washes with PBS. For immunostaining, the cells were first stained using the mouse anti-human amyloid-β mAb clone 6E10 (1:100; SIG-39320; Covance), rat anti-CD68 mAb clone FA-11 (1:100; ab53444; Abcam), rat anti-CD36 mAb clone MF3 (1:200; ab80080; Abcam), rat anti-CD204 scavenger receptor type I/II (SCARA1) mAb (1:100; MCA1322; AbD Serotec), rabbit anti-CD163 pAb (1:100; orb13303; Biorbyt), and goat anti-MMP-9 pAb (1:100; AF909; R&D systems). Secondary polyclonal antibodies included donkey anti-mouse, anti-rat, anti-rabbit, and anti-goat conjugated with Cy2, Cy3 or Cy5 (1:200; Jackson ImmunoResearch Laboratories). The

cells were mounted using ProLong® Gold with DAPI (Molecular Probes, Life Technologies). Several fields (minimum $n = 5$ randomly selected per group) were obtained from each well using a Carl Zeiss Axio Imager Z1 ApoTome-equipped microscope (an average of 120 cells in each field). Images were obtained using the same exposure time in each occasion. The fluorescent signal and its total area were determined and quantified by the conversion of individual images to greyscale and standardizing to baseline using histogram-based thresholds with NIH ImageJ software. The 'mean area per cell' was a result of a numerical average of the individual cell's immunoreactive area per field. The 'area/cell' measures the total fluorescent signal (area) divided by the total number of cells (DAPI count) of the same field (image). For all experiments, the investigators were blinded to the treatment condition.

Statistical analysis

GraphPad Prism 6.01 (GraphPad Software) was used to analyse the data. A comparison of two or more groups during several days (Barnes maze test) was performed using a two-way ANOVA followed by the Bonferroni multiple comparison post-test of paired groups. A comparison of three or more groups was performed using a one-way ANOVA followed by the Tukey or Bonferroni multiple comparison test of paired groups. Two-group comparisons were analysed using a two-tailed unpaired Student *t*-test. StatPlus paired *t*-tests and one-way ANOVA with Tukey *post hoc* comparisons were conducted for quantification of the synaptic area. Correlation analysis was performed using Prism Pearson's tests. Results are expressed as means ± standard deviations (SDs) or means ± standard errors of the mean (SEMs) as indicated. A P-value < 0.05 was considered significant.

Results

CD115+ monocyte blood enrichment and glatiramer acetate immunization reduced cognitive deficits

Symptomatic ADtg mice (10-month-old males) were treated with subcutaneous GA injections given weekly for a period of 9 weeks, peripheral blood infusion of GFP-labelled bone marrow-derived CD115+ monocytes (Mo^{BM}; isolated from 8- to 10-week-old young donor mice) delivered to the tail vein once a month for 2 months, or both ($GA + Mo^{BM}$). The adoptive transfer of Mo^{BM} enriches the circulating blood of adult ADtg mice with this subpopulation of inflammatory monocytes by 5- to 6-fold. Mo^{BM} were derived from young donor mice with increased yield of isolated CD115+ monocytes. This procedure was shown to increase recruitment of beneficial monocyte-derived macrophages to the spinal cord in an acute injury model (Shechter *et al.*, 2009). Control groups were age- and sex-matched ADtg mice injected with PBS and untreated non-transgenic (wild-type) mice. Figure 1 depicts a description of the experimental procedure and timeline.

At the completion of the treatment period, all mice underwent behavioural testing at the age of 12 months using the Barnes maze paradigm to evaluate hippocampus-dependent spatial memory and learning (Fig. 2). The behavioural tests were assessed in two separate cohorts of mice. All observers were blinded to the treatment groups. Prior to the Barnes maze testing, an open field test of ambulation and rearing behaviour was performed to confirm that the mice were suitable for cognitive testing (data not shown). The first cohort of mice was used to evaluate behavioural functions following GA and combined $GA + Mo^{BM}$ treatments (Fig. 2A and B). The escape latency times decreased for all mouse groups during the 4-day training/acquisition phase ($P < 0.0001$, $F = 25$, $df = 3$, two-way ANOVA between days; $n = 7$ mice/group; Fig. 2A), with no significant difference between experimental groups on Days 1–3. However, on Day 4, GA and $GA + Mo^{BM}$ mice displayed a trend of decreased latency time when compared to PBS control ADtg mice, and the latency time did not differ from that of the wild-type mice. The latter group showed a significantly shorter mean latency than the PBS ADtg group (Fig. 2A). A memory retention test was performed after a 2-day break (Day 7). A one-way ANOVA showed no significant differences in mean latencies between the treatment groups and the PBS group (Fig. 2A, middle graph), while there were significantly shorter latency times in the wild-type group when compared with both the GA and PBS groups ($P < 0.05$). The $GA + Mo^{BM}$ group displayed a trend of shorter latency with no significant difference from that of the wild-type group. During the reversal phase, Days 8 and 9, the location of the escape box was altered. A two-way ANOVA showed highly significant differences between both treatment groups and the PBS control group ($P < 0.0001$, $F = 13.08$, $df = 3$). One-way ANOVA of mean latencies for Day 9 demonstrated significant differences between the PBS group and the GA group ($P < 0.05$; 53% reduction) as well as between the PBS group and the $GA + Mo^{BM}$ group ($P < 0.0001$; 74% reduction), with mean latencies in the combined treatment group ($GA + Mo^{BM}$) essentially indistinguishable from those in the wild-type group (Fig. 2A, right).

An ANOVA of incorrect box entries (errors) during the 4-day acquisition phase revealed significant differences between all groups ($P < 0.0001$, $F = 9.4$, $df = 3$; Fig. 2B), especially on Day 4 of the training phase ($P = 0.0042$, $F = 5.7$, $df = 3$), when the GA and $GA + Mo^{BM}$ groups differed from the PBS control group ($P < 0.05$). Error counts overall decreased between Days 1 to 4 ($P = 0.0191$, $F = 3.5$, $df = 3$). Both treated ADtg mouse groups were not significantly different from the wild-type group (Fig. 2B, left) with respect to this measure. An analysis of errors in the memory retention test on Day 7 revealed significantly fewer errors in both the GA and $GA + Mo^{BM}$-treated ADtg mice groups when compared with the PBS controls ($P = 0.0017$ between groups and $P < 0.05$ according to Tukey's multiple comparison post-test for the GA and

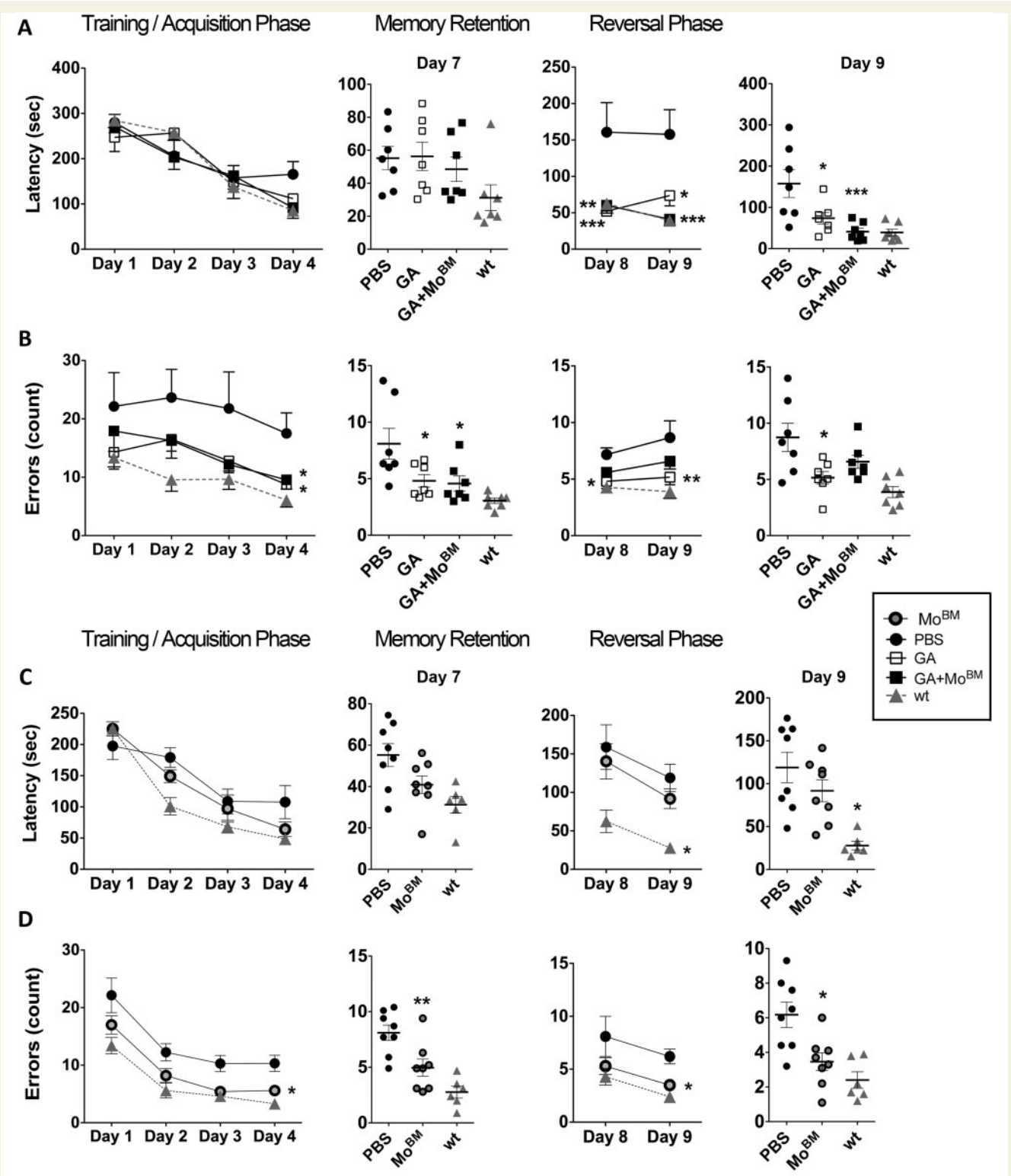

Figure 2 Reduced spatial learning and memory deficits in treated ADtg mice as assessed using the Barnes maze test. (**A** and **B**) The first cohort of PBS-injected, GA-immunized, and GA plus Mo^{BM}–treated ADtg mice were assessed for cognitive function when the animals were 12.5 months old ($n = 7$ mice/group). An additional control group composed of age- and sex-matched untreated non-transgenic (wild-type, wt) mice ($n = 7$) was also tested. During the training/acquisition phase, all mouse groups became more efficient in finding the escape box, resulting in a reduced escape latency (Latency; **A**) and fewer incorrect entries (Errors; **B**). A two-way ANOVA showed no significant difference in mean latency between the treatment groups but a highly significant difference ($P < 0.0001$) between Days 1 and 4 (**A**, *left*). The same analysis indicated significant differences in the mean number of errors: $P < 0.0001$ between treatment groups and $P = 0.0191$ between Days 1 and 4 days (**B**, *left*). An analysis of individual days (Days 1–4) by one-way ANOVA showed no significant differences for latency (**A**), but indicated a significant reduction in the number of errors (**B**) in the treated groups compared to the PBS control group. A memory retention test was performed after a

(continued)

GA + Mo^{BM} groups compared with the PBS group). Importantly, the performances of both treatment groups were not significantly different from that of the non-transgenic, age-matched wild-type group (Fig 2B, middle graph). In the reversal phase, Days 8 and 9, significant differences were observed between the experimental groups ($P < 0.0001$, F = 9.334, df = 3; two-way ANOVA). The reduction in mean errors on Day 9 reached significance for the GA group relative to the PBS control group ($P < 0.05$ with a 41% reduction), and this was not significantly different from the mean errors in the wild-type mice (Fig. 2B, right).

To test whether blood enrichment of monocytes alone is beneficial in reducing behavioural deficits in animal models of Alzheimer's disease, we repeated the experiment described above using three groups and compared the Mo^{BM} group to the PBS control group and untreated wild-type mice. Mice were assessed at the same age as the first cohort by performing the Barnes maze test ($n = 8$ mice each in the Mo^{BM} and PBS groups and $n = 6$ in the wild-type mouse group; Fig. 2C and D). During Days 1–4 of training/acquisition, significant reductions were detected in both latency ($P = 0.0104$, F = 4.854; df = 2 between groups; and $P < 0.0001$, F = 41.32, df = 3 between Days 1–4; two-way ANOVA) and errors ($P < 0.0001$, F = 22.08; df = 2 between groups; and $P < 0.0001$, F = 35.16, df = 3 between Days 1–4; two-way ANOVA; Fig. 2C and D, left). An ANOVA for Day 4 separately revealed a significant 45% reduction in the number of errors for the Mo^{BM} group compared to the PBS control group ($P = 0.0007$, F = 11.04, df = 2, with $P < 0.05$; Tukey's multiple comparison post-test).

Compared to the PBS control group, with respect to memory retention on Day 7, the Mo^{BM} group displayed a trend of reduction in latency ($P = 0.0595$; Fig. 2C), with a substantial reduction of 39% in the number of errors ($P < 0.001$, Tukey's post-ANOVA test; Fig. 2D); there was no significant difference between the Mo^{BM} and wild-type group. A significant behavioural benefit was also apparent in the reduced number of incorrect entries during the 2-day reversal phase following Mo^{BM} infusion ($P = 0.0014$, F = 7.86 between groups, and $P = 0.0266$, F = 5.33 between days; two-way ANOVA; Fig. 2D, right). No significant difference in latency times between the Mo^{BM} and PBS groups was found on Days 8 and 9 (Fig. 2C, right). On Day 9, the mean latency of the Mo^{BM} group was on average lower than PBS controls, but significantly higher than that of the wild-type group (Fig 2C, right graph; $P < 0.05$ Tukey's post-test). Importantly, in the reversal phase test performed on Day 9, a substantial improvement—a 44% reduction in the number of mean errors—was obtained in the Mo^{BM} group when compared to PBS control animals ($P = 0.0011$, F = 10.04, df = 2, with $P < 0.05$; Tukey's post-test; Fig. 2D, right). On Day 9, the mean number of errors in the Mo^{BM} mice did not differ significantly from that of the wild-type group (Fig. 2D, right). Overall, our behavioural data demonstrated that treatment of already symptomatic ADtg mice with either Mo^{BM} and/or GA had a significant effect on reducing memory and learning dysfunction in this mouse model.

Reduced cerebral amyloid-β levels and astrogliosis associated with synaptic preservation

Brain tissues were collected for histological and biochemical assessments when the animals reached the age of 13 months (Fig. 1). To study the effects of GA, the adoptive transfer of Mo^{BM}, and the combined treatment of GA + Mo^{BM} on brain pathology in ADtg mice, compared with mice given PBS, an initial evaluation of amyloid-β plaque burden was assessed in coronal brain sections (Fig. 3A–C). Representative histologic sections were found to have a substantial reduction in the hippocampal $4G8^+$ amyloid-β plaque burden in all treated groups when compared to the PBS control group (Fig. 3A). Quantitative analysis of cerebral amyloid-β plaque burden was performed on serial brain sections covering both hippocampal and cortical regions. Brain sections were immunolabelled with anti-human amyloid-β monoclonal antibody (mAb) 4G8 or fluorescently labelled with thioflavin-S (Thio-S), quantitatively assessing diffused as well as mature/fibrillar amyloid-β plaque load ($n = 7$–8 mice per group; Fig. 3B and C). Substantial 45% and 50% reductions in cerebral $4G8^+$ and Thio-S^+ plaque areas, respectively, were observed in the GA group compared to the PBS group ($P < 0.0001$ by one-way ANOVA and Tukey's

Figure 2 Continued

2-day break (on Day 7). No significant differences were observed between the treatment groups in mean latencies (**A**, *middle left*). However, the mean number of errors was significantly lower in both the GA- and GA + Mo^{BM}-treated ADtg mouse groups than in the PBS control group (**B**, *middle left*). During the reversal phase (Days 8 and 9), the location of the escape box was altered and the escape latency and errors were measured. Data analysis performed using a two-way ANOVA showed significant differences between the treatment groups and the PBS control group ($P < 0.0001$ for both latency and errors). A one-way ANOVA of mean latency on Days 8 and 9 demonstrated significant differences between the PBS group and both the GA and GA + Mo^{BM} groups. A highly significant reduction in latency was observed in the combined treatment group (GA + Mo^{BM}), which is essentially indistinguishable from the wild-type group (**A**, right graphs). However, the reduction in the number of mean errors reached significance only for the GA group, which was not significantly different from the wild-type control group (**B**, *right*). (**C** and **D**) The second cohort, which consisted of PBS control and Mo^{BM}-treated ADtg mice as well as naïve wild-type mice, was also assessed by performing the Barnes maze test when the animals were 12.5 months old ($n = 6$–8 mice/group). The data indicated that the adoptive transfer of Mo^{BM} to the peripheral blood in ADtg mice significantly reduced cognitive deficits (as shown by mean errors) for Days 4, 7 and 9. The data from individual mice as well as the group means and SEMs are shown. $^*P < 0.05$, $^{**}P < 0.001$, $^{***}P < 0.0001$.

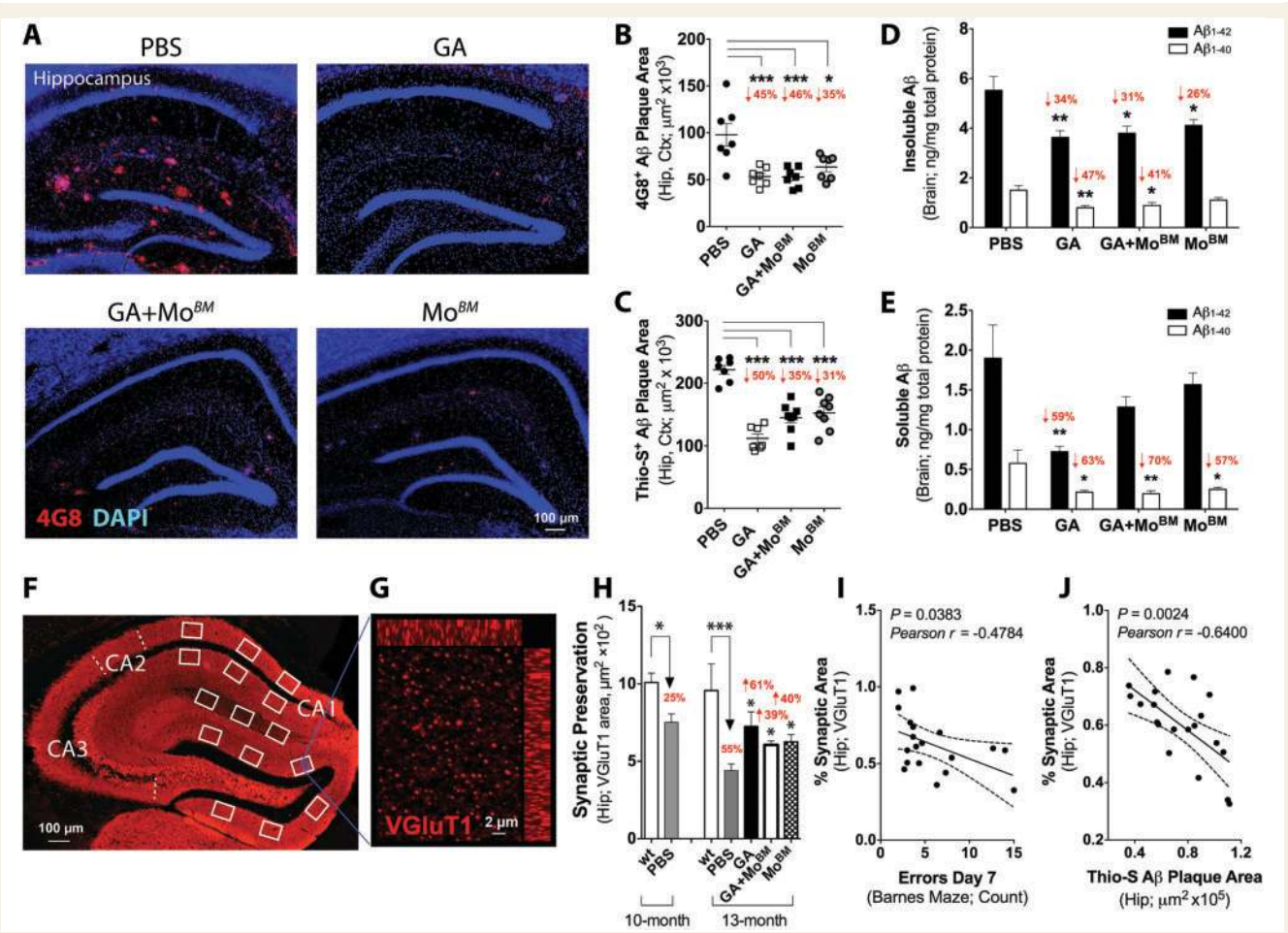

Figure 3 Decreased cerebral amyloid-β levels and increased synaptic preservation. (**A**) Representative microscopic images of coronal brain sections from 13-month-old ADtg mice from all treated groups display a reduced hippocampal plaque burden when compared to those from the PBS control group. Sections were immunolabelled with the anti-human amyloid-β monoclonal antibody 4G8 (red) and counterstained with DAPI (blue) to detect nuclei. (**B**) Quantitative immunohistochemical analyses of brain sections were assessed for 4G8-positive amyloid-β plaque area. (**C**) Quantitative analyses of brain sections assessed for thioflavin-S (Thio-S)-positive amyloid-β plaque area. In **B** and **C** all treatment groups show substantial decreases in amyloid-β plaque burden in brain regions covering the hippocampus (Hip) and cortex (Ctx). (**D**) ELISA analyses of insoluble human amyloid-β_{1-40} and amyloid-β_{1-42} in the brain indicate significant reductions in mean levels across all treatment groups compared to the PBS control group. The trend of reduction in insoluble amyloid-β_{1-40} in the Mo^{BM} did not reach statistical significance. (**E**) ELISA analyses of soluble human amyloid-β_{1-40} and amyloid-β_{1-42} in the brain. Compared to the PBS control group, all treatment groups show significant reductions in mean levels of soluble amyloid-β_{1-40}, and the GA-immunized group displays a substantial reduction in soluble amyloid-β_{1-42} levels in the brain. (**F**) Illustration of the presynaptic marker VGluT1 area measurement in the hippocampus. Fifteen fields were precisely selected in the hippocampus, and for each field, 15 optical section images were acquired and analysed. (**G**) A representative high-magnification *Z*-stack micrograph was obtained from the molecular layer of the dentate gyrus, which was immunostained with VGluT1 in the GA treatment group. (**H**) Quantification of total hippocampal synaptic areas obtained from animals in the PBS, GA, GA + Mo^{BM}, Mo^{BM}, and wild-type mouse groups. At the age of 10 months PBS-treated ADtg mice had a mild but significant loss of synaptic area (25%) compared to matched wild-type controls. In 13-month-old ADtg mice a substantial 55% synaptic area loss was observed. Significant synaptic preservation was seen for all treatment groups (39–61%) at the age of 13 months. The mean synaptic area in the GA group reached the level observed in 10-month-old PBS control ADtg mice. No significant differences were found between any of the treatment groups. (**I**) A negative correlation was noticed between the synaptic area in the hippocampus and the Barnes maze scores, specifically with respect to the number of incorrect entries in the memory retention test (Errors Day 7). A larger synaptic area in the hippocampus correlated with fewer errors indicating less cognitive deficit. (**J**) Negative correlation was found between the per cent synaptic area and the Thio-S amyloid-β plaque area in the hippocampus. Increased Thio-S^+ plaque was associated with synapse loss. Correlation analyses were performed using the Pearson's test. Data from individual mouse as well as group means and SEMs are shown. The per cent reductions or elevations in mean values, as compared with PBS controls, are indicated in red. n = 6–8 mice per group. $^*P < 0.05$, $^{**}P < 0.001$, $^{***}P < 0.0001$. Aβ = amyloid-β.

post-test; Fig. 3B and C). Similar decreases were observed when hippocampal and cortical regions were analysed separately (Supplementary Fig. 1A and B). Significant reductions of 31–46% in the 4G8$^+$ or Thio-S$^+$ plaque area were also found in the GA + Mo^{BM} and Mo^{BM} groups (Fig. 3B and C). Substantial reductions of 40–53% (hippocampus) and 61–78% (cortex) in the Thio-S$^+$ plaque number were also observed for all treatment groups ($P < 0.0001$–0.001; Supplementary Fig. 1B).

Brain insoluble and soluble amyloid-$\beta_{1–40}$ and amyloid-$\beta_{1–42}$ levels, assessed by quantitative ELISA analysis, also indicated significant differences between the experimental groups (Fig. 3D and E). Levels of insoluble amyloid-$\beta_{1–40}$ were significantly decreased: 47% in the GA group ($P < 0.001$) and 41% in the GA + Mo^{BM} group ($P < 0.05$) compared to PBS controls (Fig. 3D, white bars). The trend in the reduction of insoluble amyloid-$\beta_{1–40}$ in the Mo^{BM} group did not reach statistical significance (Fig. 3D). There were also significant reductions in brain levels of insoluble amyloid-$\beta_{1–42}$, 26–34%, in all treatment groups compared to PBS controls (Fig. 3D, black bars). Levels of soluble amyloid-$\beta_{1–40}$ were significantly reduced across all experimental groups, 57–70%; and a substantial 59% reduction in soluble amyloid-$\beta_{1–42}$ was found in GA-treated mice compared to findings in PBS control mice ($P < 0.001$–0.05, Tukey's multiple comparison post-ANOVA test; Fig. 3E). A reduction in mean brain levels of soluble amyloid-$\beta_{1–42}$ isoform was also found in the GA + Mo^{BM} and Mo^{BM} groups, although this trend did not reach statistical significance (Fig. 3E, black bars). Under these experimental conditions, GA appears to have the greatest effect in reducing cerebral amyloid-β levels. However, no significant differences were found between any of the treatment groups; instead, the only significant differences we observed were between the treatment groups and the PBS controls. Although no synergistic effects on amyloid-β pathology were observed in the combined GA + Mo^{BM} group, it is important to note that the reduction in soluble amyloid-$\beta_{1–40}$ isoform, which is the most frequent form of amyloid-β deposited in blood vessel walls, was the greatest change found in this treatment group (Fig. 3E, white bars).

To assess the effect of immune modulation on synaptic preservation, we analysed the presynaptic marker vesicular glutamate transporter 1 (VGluT1) area in the hippocampus (Fig. 3F–H). Fifteen high-magnification *Z*-stack images from 15 hippocampal fields were selected and analysed for VGluT1 in the hippocampus, covering areas such as the molecular layer of the dentate gyrus and the cornu ammonis 1 (CA1) (Fig. 3F). Representative *Z*-stack images from PBS, GA and wild-type groups are shown in Supplementary Fig. 2A–C. An enlarged *Z*-stack and high-magnification image from a GA-immunized mouse brain is shown in Fig. 3G. A quantitative analysis revealed a substantial loss of hippocampal presynaptic VGluT1-immunoreactive area (55%) in PBS-treated ADtg control mice, as compared to aged-matched wild-type mice ($P < 0.0001$), while significant synaptic preservation of 39–61% was observed in all treatment groups ($P < 0.05$; Fig. 3H; $n = 6$ mice per group). GA exhibited the greatest increase in the hippocampal presynaptic VGluT1 area (Fig. 3H). In a younger cohort of symptomatic animals (at 10 months old, $n = 6$), the synaptic area in PBS-treated ADtg mice was significantly reduced (25%) compared to wild-type mice ($P < 0.05$, Fig. 3H). Note, a substantial decrease in synaptic area was also observed in 10-month-old versus 13-month-old PBS-control ADtg mice ($P = 0.0035$, Fig. 3H), with disease progression. Importantly, this loss of hippocampal synaptic area in the 13-month-old ADtg mice was reversed following GA immunization to the mean synaptic area levels of 10-month-old control ADtg mice (Fig. 3H). Correlation analyses at the individual mouse level indicated a significant negative correlation between the per cent synaptic area and Barnes maze error scores obtained on Day 7 (memory retention) as well as between the per cent synaptic area and the Thio-S$^+$-amyloid-β plaque area in the hippocampus ($P = 0.002$–0.038 by Pearson's test; Fig. 3I and J, and Supplementary Fig. 2D). These correlation analyses predicted that a larger presynaptic VGluT1 area is associated with better cognitive scores and with decreased Thio-S$^+$ plaque in the hippocampus. Accordingly, a loss of presynaptic area in the hippocampus correlated with increased errors indicative of a cognitive deficit and with an increased Thio-S$^+$ plaque area (Fig. 3I and J, and Supplementary Fig. 2D).

In Alzheimer's disease, astrocytes accumulate in response to amyloid-β plaque lesion sites and exhibit increased reactivity and cytotoxicity, namely, astrocytosis or astrogliosis (Cairns *et al.*, 1992; Kato *et al.*, 1998; Akiyama *et al.*, 2000*a*; Wyss-Coray and Mucke, 2002; Kamphuis *et al.*, 2014). We found that GA and monocyte enrichment reduced astrogliosis, as assessed by the decreased expression of astrocyte-specific glial fibrillary acidic protein (GFAP; Fig. 4). Representative micrographs show a marked reduction in both the number of, and overall area occupied by, GFAP$^+$ astrocytes in the GA group (Fig. 4A). In the PBS group, GFAP$^+$ astrocytes were tightly associated with 4G8$^+$-amyloid-β plaques and frequently had a structure reminiscent of reactive astrocytes, which are typical of inflammatory Alzheimer's disease pathology. On the contrary, in treated mice, along with reduced GFAP$^+$ astrogliosis, more astrocytes exhibited a resting morphology as observed in the brains of wild-type animals (Fig. 4A).

Quantitative immunohistochemical analyses of GFAP$^+$ cell number and total area were performed in a subgroup of mice from each experimental group ($n = 4$–5 mice/group). This analysis indicated that the three types of immune-modulation treatments significantly reduced levels of cortical astrogliosis ($P < 0.0001$ between all groups, one-way ANOVA with Tukey's multiple comparison post-tests; Fig. 4B and C). Similar quantitative data were obtained in the hippocampal area (data not shown). Again, GA appeared to have the strongest effect on reducing mean cortical GFAP$^+$ cell numbers and area (49% and 77%,

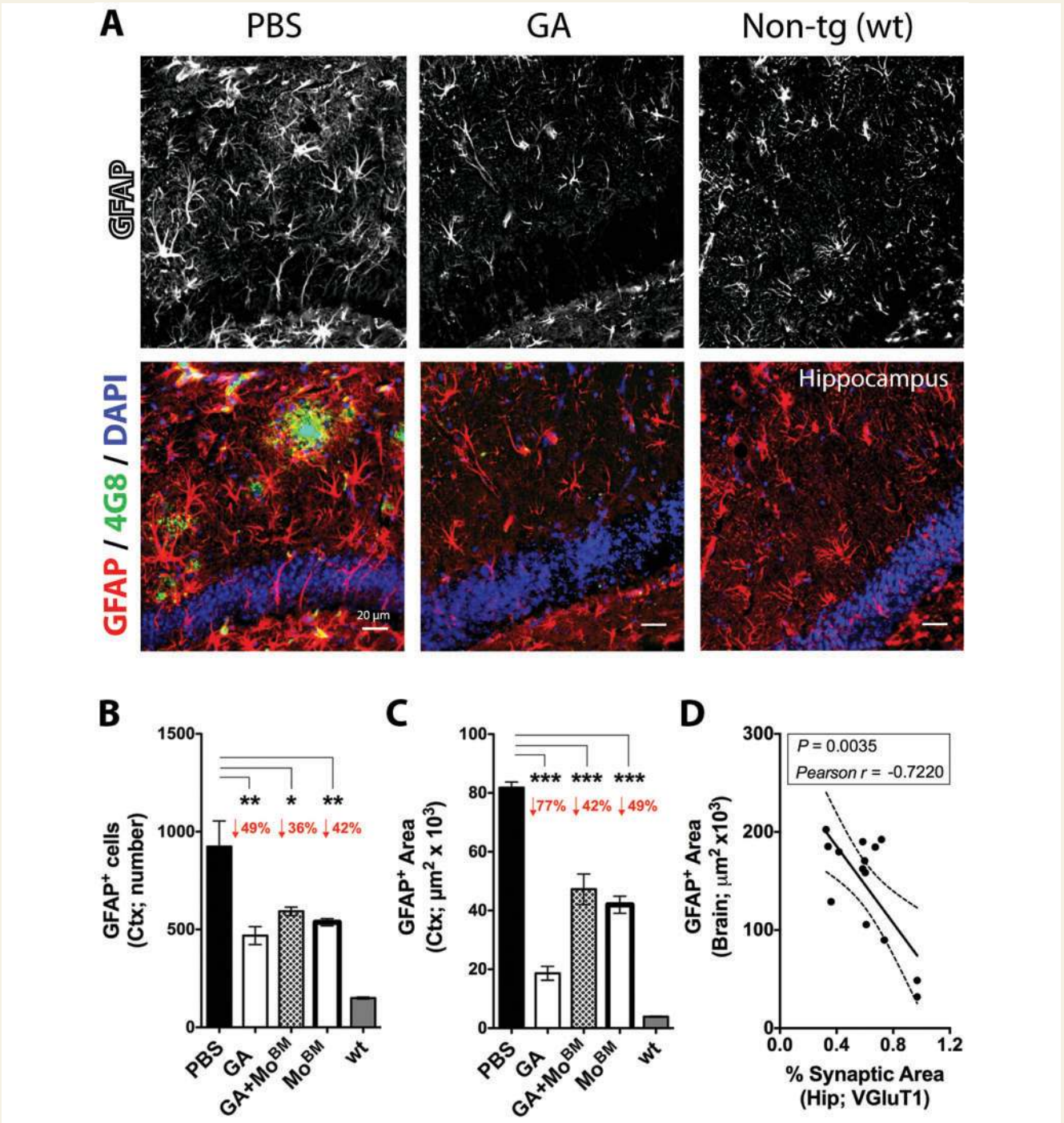

Figure 4 Reduction in cerebral GFAP$^+$ astrogliosis. Brain coronal sections from 13-month-old ADtg and non-transgenic (non-tg, wild-type, wt) mice were co-labelled with the anti-human amyloid-β antibody (4G8; green) and the astrocyte-specific GFAP antibody (red). Sections were counterstained with DAPI (blue) to detect nuclei. (**A**) Representative fluorescence micrographs of hippocampal regions depict reduced staining for GFAP in GA-immunized ADtg mice compared to PBS controls; staining in the treated group is similar to that in tissue from the wild-type brain. For simplicity of viewing, the upper portion of **A** shows the single GFAP channel as greyscale. (**B** and **C**) Quantitative immunohistochemical analysis of GFAP$^+$ cell number and area across all experimental groups. (**B**) The three types of immune-modulation treatment were found to substantially reduce cortical astrocytosis levels ($P < 0.001$–0.05), and there is no significant difference in the astrocyte cell count between the treatment groups. (**C**) GA therapy appears to have the largest effect on reducing the mean cortical GFAP$^+$ area ($P < 0.0001$ between GA and either the Mo^{BM} or GA + Mo^{BM} groups). Cortical astrogliosis levels in all treatment groups are significantly higher than levels found in the wild-type group. (**D**) Negative correlations were perceived between the per cent synaptic area and cerebral GFAP+ immunoreactivity in the brain. Correlation analyses were performed using the Pearson's test. Group means and SEMs are shown. The percentage reductions in mean astrocyte number and total area in GA, Mo^{BM}, and combined GA + Mo^{BM}-treated animals, compared to PBS control mice, are indicated in red. $n = 3$–5 mice per group. *$P < 0.05$, **$P < 0.001$, ***$P < 0.0001$.

respectively), yet the difference between the GA group and the monocyte-treated groups reached statistical significance only for the analysis of GFAP$^+$ area ($P < 0.0001$, Tukey's post-test; Fig. 4C). The extent of cortical astrogliosis in all treatment groups, although substantially reduced compared with that in the PBS group, was still significantly higher than the extent found in the wild-type group ($P < 0.001$ for the GA group and $P < 0.0001$ for the Mo^{BM} and the GA + Mo^{BM} groups; Fig. 4B and C). No significant differences were found between the two monocyte-treated groups (Mo^{BM} versus GA + Mo^{BM}). Overall, no additive or synergistic beneficial effect was observed for combining GA and monocyte treatment with respect to astrogliosis or amyloid-β levels. An analysis of individual mouse values indicated a strong negative correlation between per cent presynaptic area and the GFAP$^+$ area in the hippocampus, indicating a strong link between astrogliosis and loss of synapses ($P = 0.0024$; Fig. 4D), especially in the molecular layer of the dentate gyrus ($P < 0.0001$; Supplementary Fig. 2E).

Increased recruitment of monocyte-derived macrophage to cerebral amyloid-β plaques

We next tested whether the beneficial effects of GA immunization (Figs 2–4) were associated with an increased spontaneous recruitment of monocyte-derived macrophage to amyloid-β deposition sites in the brain. We used three methods to assess recruitment of monocyte-derived cells to the brain: (i) detection of blood-injected GFP-labelled monocytes; (ii) histological analysis of distinctive expression levels of the surface marker CD45 in resident microglia, as opposed to monocyte-derived macrophage, combined with the surface marker ionized calcium binding adapter molecule 1 [Iba1$^+$/CD45^{high} macrophage versus Iba1$^+$/CD45$^{int/low}$ resident microglia (Ford *et al.*, 1995; Renno *et al.*, 1995; Juedes and Ruddle, 2001; Koronyo-Hamaoui *et al.*, 2009; Prinz *et al.*, 2011)]; and (iii) flow cytometry analysis of mononuclear-enriched cells from whole brains gated for CD11b$^+$/CD45^{high}/Ly6C^{high} inflammatory monocytes (Prinz *et al.*, 2011). The histological examination of large series of coronal brain sections revealed the presence of GFP-labelled, peripherally injected bone marrow-derived CD115$^+$/CD45^{high} cells adjacent to amyloid-β plaques (Fig. 5A). Spontaneous recruitment of the GFP-macrophage subpopulation to cerebral amyloid-β depositions was clearly evident in both ADtg mouse groups following blood enrichment of Mo^{BM} with or without GA immunization. GA further increased GFP-macrophage recruitment, as qualitatively observed in the combined GA + Mo^{BM} group when compared with the Mo^{BM} group (Fig. 5A). No cerebral infiltration of monocytes was detected in a cohort of non-transgenic (wild-type) mice that received adoptive transfer of GFP-Mo^{BM} (data not shown).

In the PBS-treated control ADtg mice brains, larger and highly aggregated amyloid-β plaques were frequently associated with activated microglial cells (Iba1$^+$/CD45$^{int/low}$) and much less with Iba1$^+$/CD45^{high} cells, which were indicative of infiltrating macrophage (Fig. 5B). As a result of GA immunization, and, moreover, in the combined GA + Mo^{BM} group, a high number of Iba1$^+$/CD45^{high} cells were observed surrounding hippocampal amyloid-β plaques (Fig. 5C). There was co-localization of Iba1$^+$/CD45^{high} macrophage cells with intracellular amyloid-β immunoreactivity, indicating cellular uptake of amyloid-β by infiltrating macrophage (Fig. 5C, inset: an arrow showing co-localization of amyloid-β in macrophage in white spots). Indeed, Iba1$^+$/CD45^{high} macrophages were found to be frequently involved in intracellular amyloid-β uptake, which was illustrated in a higher-magnification micrograph (Fig. 5C′, arrows). This result agrees with findings cited in previous reports, which suggest that cellular uptake of amyloid-β is more frequently observed among macrophage than microglia cells (Malm *et al.*, 2005, 2010, 2012). In the cortical region of brains from the GA + Mo^{BM} group, amyloid-β plaques were also generally smaller, more diffused, and tightly associated with Iba1$^+$/CD45^{high} infiltrating macrophages directly involved in intracellular amyloid-β uptake (Fig. 5D).

In the next set of experiments, we quantitated the total (GFP-injected and endogenous) monocyte infiltration by assessing the Iba1$^+$CD45^{high} macrophage–immunoreactive area and the ratio of total macrophage area to amyloid-β plaque area covering the cortical and hippocampal brain regions in all treatment groups (Fig. 5E and F, and Supplementary Fig. 3; $n = 6$–7 mice per group). An analysis of the Iba1$^+$CD45^{high} macrophage area indicated that the combined GA + Mo^{BM} treatment in particular, but also the GA and the Mo^{BM} treatments, induced cerebral recruitment of macrophage ($P < 0.05$ ANOVA with Bonferroni's post-test; Fig. 5E). Separate analyses of brain regions—cortex and hippocampus—indicated significant increases in mean areas of Iba1$^+$CD45^{high} macrophage in the hippocampus in all treatment groups, compared to the PBS group (Supplementary Fig. 3C). This trend did not reach statistical significance in the cortical region (Supplementary Fig. 3A). Enhanced hippocampal monocyte recruitment was especially evident in the GA and the combined GA + Mo^{BM} groups ($P < 0.05$ and $P < 0.001$, ANOVA with Bonferroni's post-test, respectively; Supplementary Fig. 3C). Although the difference in the Mo^{BM} group did not reach statistical significance in the multiple comparisons ANOVA and Bonferroni's post-test, a comparison of this group alone with the PBS controls resulted in a highly significant difference ($P < 0.0001$, Student *t*-test; asterisks in parenthesis; Supplementary Fig. 3C).

A ratio analysis of total macrophage area to amyloid-β plaque area, in brain regions covering the cortex and hippocampus, indicated that the Mo^{BM} and GA + Mo^{BM} groups had marked 3.1- and 4.3-fold increases in total recruited macrophage per amyloid-β plaque area, respectively ($P < 0.0001$ and $P < 0.05$; Fig. 5F). Separate cortical and hippocampal analyses show similar results (Supplementary Fig. 3B

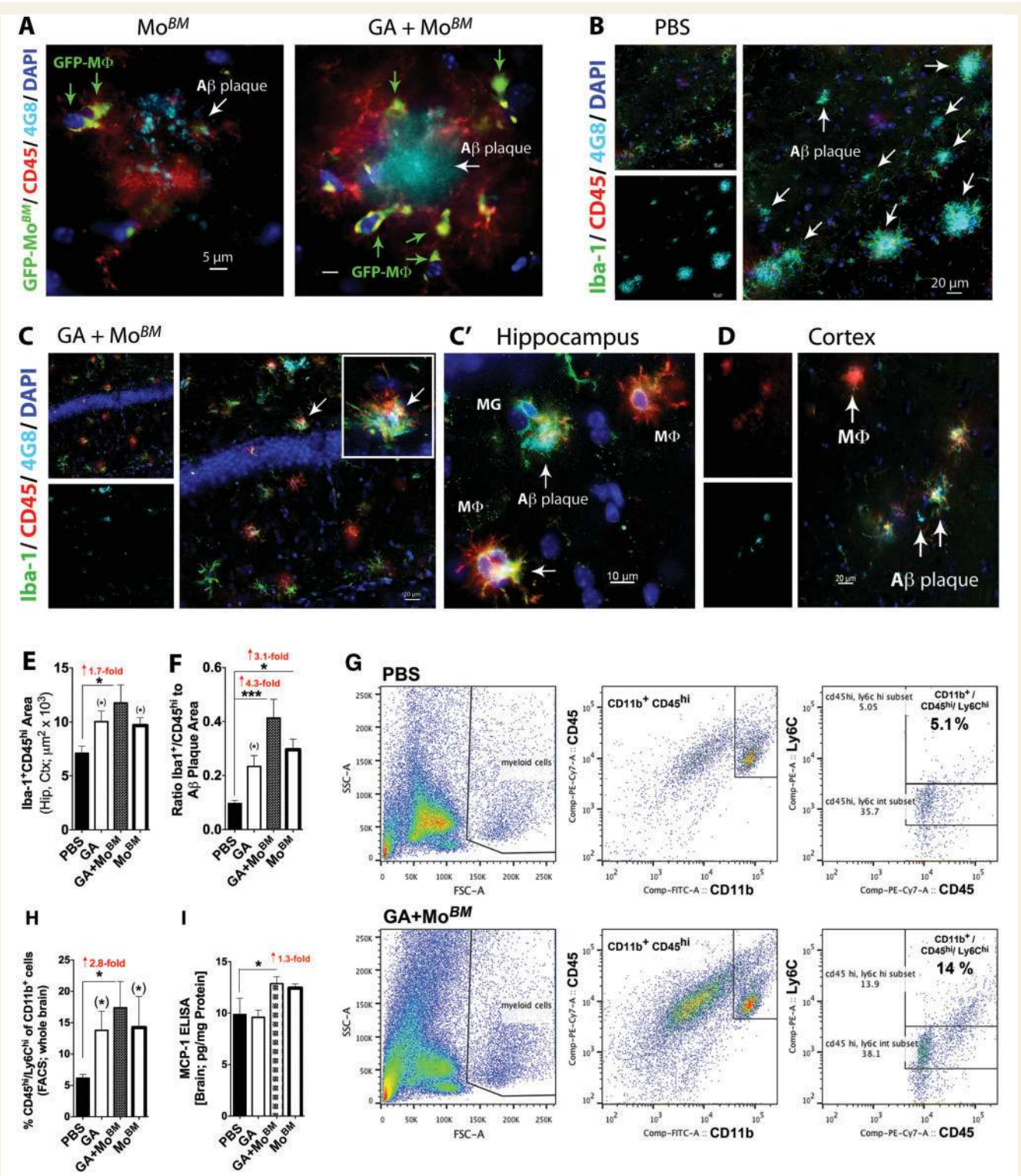

Figure 5 Enhanced infiltration of blood-borne phagocytic monocyte-derived macrophages associated with amyloid-β plaque clearance. GFP-labelled bone marrow-derived $CD11b^+CD115^+$ cells were isolated from young (8- to 10-week-old) donor wild-type mice and injected into the tail vein of symptomatic 10-month-old ADtg mice, with or without GA immunization, once a month over a period of 2 months. (**A**) Fluorescence micrographs of hippocampal coronal sections from 13-month-old ADtg mice that were immunolabelled for anti-GFP (green), CD45 (red), human amyloid-β (4G8; cyan), and nuclei (DAPI, blue). Spontaneous recruitment of GFP-labelled monocyte-derived macrophages from the peripheral blood to amyloid-β deposition sites was found in both GA-immunized and non-immunized ADtg mice in which adoptive transfer of Mo^{BM} occurred. An additional increase in recruitment of GFP-labelled monocytes to the brain was observed in the combined GA + Mo^{BM} group compared to the non-immunized Mo^{BM} group. (**B–D**) Additional immunolabelling distinguishes between resident microglia ($Iba1^+/CD45^{int/low}$) and monocyte-derived macrophage ($Iba1^+/CD45^{high}$). Composite pictures and images from individual colour channels are

(continued)

Table 1 Manual count of Iba1$^+$CD45^{high}-macrophage cells and their ratio to plaque number in brain regions covering the hippocampus and cortex in all treatment groups

Treatment	Brain area	CD45^{hi} (Iba1$^+$) cell[a]			Ratio CD45^{hi} cell[a]/amyloid-β plaque[a]		
		Mean	STD	*P*-value (versus PBS)	Mean	STD	*P*-value (versus PBS)
PBS	Cortex	10.1	2.9		0.4[b]	0.1	
GA	Cortex	9.7	4.4	NS	0.7	0.3	0.0296[c]
GA + Mo^{BM}	Cortex	13.0	2.4	0.0356[c]	0.9	0.4	0.0071[c]
Mo^{BM}	Cortex	9.7	2.2	NS	0.8	0.2	0.0019[c]
PBS	Hippocampus	5.8[b]	2.0		0.3	0.1	
GA	Hippocampus	6.3	2.9	NS	0.4	0.2	NS
GA + Mo^{BM}	Hippocampus	11.7	3.8	0.0026[c]	0.8	0.6	0.0287[c]
Mo^{BM}	Hippocampus	7.7	1.0	0.0265[c]	0.7	0.2	0.0037[c]

[a]Number of cells and plaques: $n = 6–8$ mice/group.
[b]$P < 0.05$ by one-way ANOVA in comparison between all four treatment groups.
[c]$P < 0.05$ by Tukey's multiple comparison post-ANOVA test.
NS = not significant.

and D). GA immunization alone also significantly increased macrophage recruitment associated with amyloid-β plaque in both brain regions together and separately ($P < 0.05$ in cortex and $P < 0.001$ in hippocampus, Student *t*-test; Fig. 5F and Supplementary Fig. 3B and D).

An independent quantitative immunohistochemical assessment of our data, by another observer also blinded to the identity of the mouse groups, involved counting the number of infiltrating Iba1$^+$CD45^{high}-macrophage and the number of amyloid-β plaques in the cortex and hippocampus in animals of all treatment groups. The results are presented in Table 1 and essentially validate our previous results shown in Fig. 5E and F, and Supplementary Fig. 3A–D. These data indicated that in brains of animals treated with GA + Mo^{BM}, compared with brains of animals given PBS (control), on average 13 (versus 10) cortical macrophage and 12 (versus 6) hippocampal macrophages were detected for each field that covered a 0.15-mm^2 area ($n = 24$ fields/brain). A ratio analysis of infiltrating macrophage per amyloid-β plaque numbers indicated the highest presence of macrophage associated with plaque in the GA + Mo^{BM} group (Table 1). While in the PBS group there is on average one recruited macrophage for every 2.5 cortical and three hippocampal plaques, in the GA + Mo^{BM} group there is one recruited macrophage for every 1.2 cortical and 1.6 hippocampal plaques ($P < 0.01$ and $P < 0.05$ in cortex and hippocampus, respectively; one-way ANOVA and Tukey's multiple comparison post-test; Table 1). In addition, each treatment approach—GA treatment and Mo^{BM} therapy—separately appeared to increase

Figure 5 Continued
presented. In PBS control brains (**B**), the amyloid-β plaques are larger, highly aggregated, and mostly associated with activated microglial cells (Iba1$^+$/CD45$^{int/low}$; green). In GA + Mo^{BM}-treated brains (**C**), the amyloid-β plaques are generally smaller, more diffused, and highly associated with Iba1$^+$/CD45^{high} infiltrating monocyte-derived macrophage (red). *Inset*: an arrow showing co-localization of amyloid-β in macrophage in white spots. A higher-magnification image of the area depicted in **C** is seen in **C′**. Both microglia (MG) and macrophages (MΦ) are found at amyloid-β plaque sites in the hippocampus of GA + Mo^{BM}-treated brains. There is co-localization of Iba1$^+$/CD45^{high} cells and intracellular amyloid-β immunoreactivity, indicating cellular uptake of amyloid-β. Cellular uptake of amyloid-β is more frequently observed among macrophage than among microglia cells (**C** and **C′**). A similar increase in infiltrating Iba1$^+$/CD45^{high} macrophages in the treated groups was also found in cortical regions (**D**). (**E** and **F**) Quantitation of the Iba1$^+$CD45^{high}-macrophage immunoreactive area (**E**), the ratio of infiltrating macrophage area per 4G8$^+$-amyloid-β plaque area (**F**), and a table presenting a manual count of Iba1$^+$CD45^{high}-macrophage cells and their ratio to plaque number (Table 1) in brain regions covering the hippocampus and cortex in all treatment groups. All treatment groups showed increases in cerebral macrophage recruitment associated with amyloid-β plaques; especially, the GA + Mo^{BM}-treated brains, which showed a marked increase in macrophage recruitment to the hippocampal and cortical regions (**E**) and association with plaque lesion sites (**F**). Similar results are observed by a manual count of infiltrating cells and individual plaque numbers (Table 1). (**G** and **H**) An additional cohort of 10-month-old ADtg mice received GA-immunizations, with or without an injection of Mo^{BM}, or PBS injections ($n = 4–6$ mice/group) for a month. Thirty-six hours after completion of the treatment period, the brains were perfused before harvest and mononuclear cells from whole brains were enriched on a Percoll® gradient. (**G**) Representative graphs of flow cytometric analysis from PBS (*top*) and GA + Mo^{BM}-treated (*bottom*) groups. Infiltrating cells were defined as CD11b$^+$CD45^{high}. The CD11b$^+$CD45^{high} cells were further gated for Ly6C^{high} for quantification of infiltrating inflammatory monocytes. (**H**) Quantitative flow data showing the percentage of total CD11b$^+$ cells that are also CD45^{high}Ly6C^{high}. These data indicate that more inflammatory monocytes (CD45^{high}Ly6C^{high}CD11b$^+$) are present in the brains of all treated ADtg mouse groups than in the PBS group. This trend is especially significant for the GA + Mo^{BM}-treated group. (**I**) ELISA measurements of soluble MCP1 (CCL2) in the brains of all mouse groups. Group means and SEMs are shown, and the mean fold increase is indicated in red. $n = 6–7$ mice per each group for the first cohort and $n = 4–6$ mice per group for the second mouse cohort. *$P < 0.05$, **$P < 0.001$, ***$P < 0.0001$, ANOVA and Bonferroni's post-test, while the smaller asterisks in parentheses signify a two-group comparison using the unpaired two-tailed Student *t*-test. Aβ = amyloid-β.

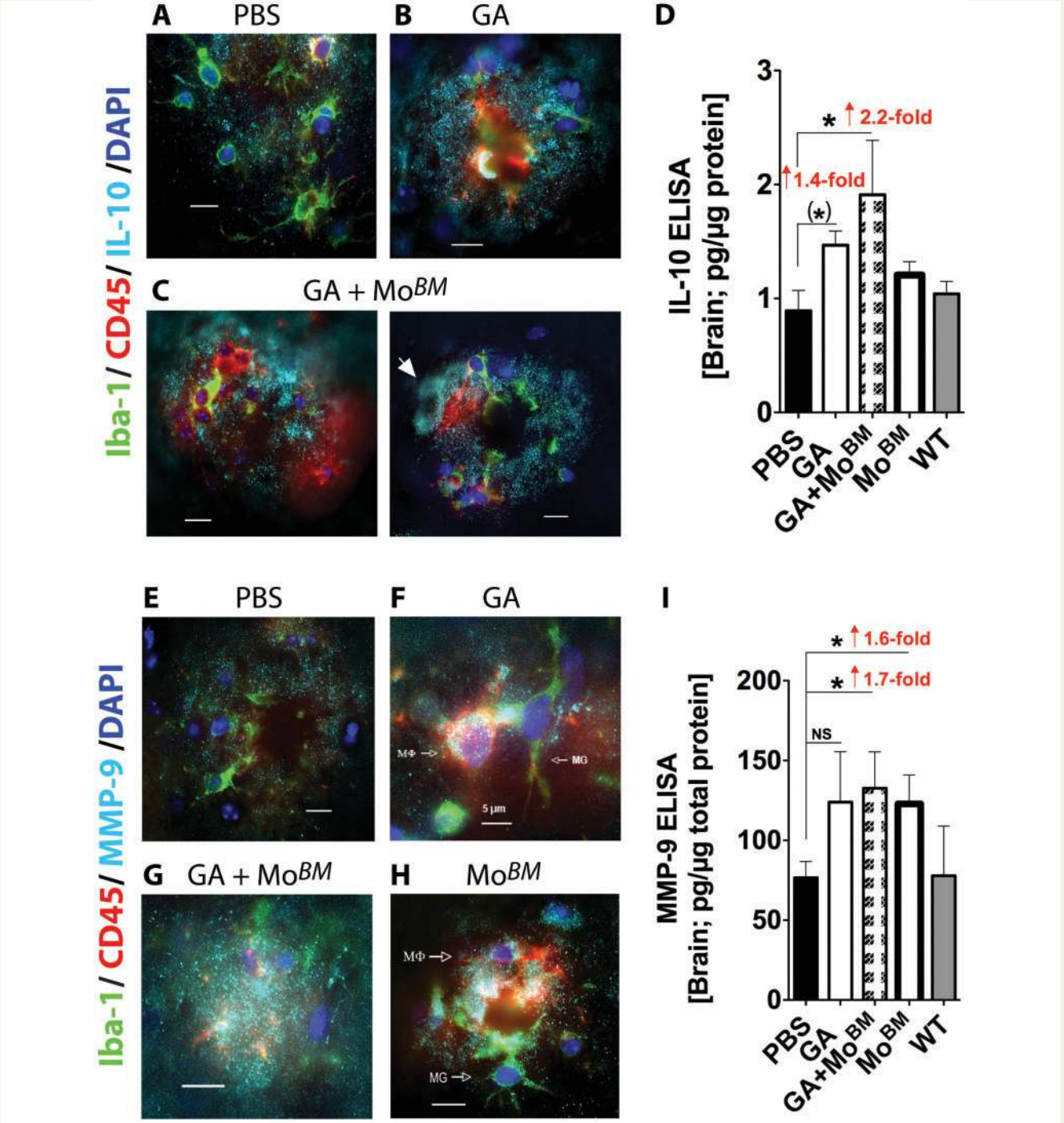

Figure 6 GA induces IL10 and MMP9 surrounding cerebral plaque. Coronal brain sections from 13-month-old ADtg mice, either treated or given PBS, were co-labelled with a combination of the markers Iba1 (green) and CD45 (red), to detect resident microglia ($Iba1^{+}$/$CD45^{int/low}$) and monocyte-derived macrophage ($Iba1^{+}$/$CD45^{high}$), and with the anti-IL10 antibody (cyan). Sections were counterstained with DAPI to detect nuclei (blue). (**A–C**) Representative fluorescence micrographs indicate low levels of IL10 expression in PBS control brains, whereas elevated IL10 levels (expressed by microglia and monocytes) are observed in GA- and GA + Mo^{BM}–treated brains. IL10 was found to be concentrated around plaque lesion sites (data not shown). Note: In the GA and GA + Mo^{BM} groups (**C**, right image), IL10 was also found to be highly expressed by non-myelomonocytic $CD45^{-}$/$Iba1^{-}$ cells (possibly astrocytes and oligodendrocytes). (**D**) Quantitative ELISA analysis of IL10 levels in brain samples showed a substantial increase in IL10 in GA + Mo^{BM}-treated ADtg mice (2.2-fold increase in mean levels) compared to control animals given PBS. The GA group had a 1.4-fold increase in IL10, compared to the PBS group, reaching significance only with the Student *t*-test. This trend did not reach significance for the Mo^{BM} group. There were no significant differences between treated groups and the untreated wild-type group. (**E–H**) Coronal brain sections from all mouse groups were co-labelled with a combination of the markers Iba1 (green), CD45 (red), MMP9 (cyan), and DAPI (blue) for nuclei. (**E**) Representative fluorescent micrograph indicates basal MMP9 levels in the brains of PBS control ADtg mice, whereas increased amounts of MMP9 were frequently found in the brains of GA-, Mo^{BM}-, and GA + Mo^{BM}-treated animals (**F–H**). This

(continued)

the recruitment of macrophage associated with amyloid plaques (Table 1).

These data were further validated by a quantitative flow cytometry analysis of whole brains isolated from another cohort of 11-month-old ADtg mice that had received identical treatments for a 1-month period starting at the age of 10 months (Fig. 5G and H). Representative flow cytometric scatter plots from PBS and GA + Mo^{BM}-treated groups indicate gating for $CD11b^+CD45^{high}$ cells and further gating for infiltrating inflammatory monocytes as $CD45^{high}/Ly6C^{high}$ of $CD11b^+$ cells (Fig. 5G). Quantification of these cells as a percentage of $CD11b^+CD45^{high}$ cells indicated a significant increase in inflammatory monocytes ($CD45^{high}Ly6C^{high}CD11b^+$) present in the brains of all treated groups, compared to the PBS group ($P < 0.05$ by one-way ANOVA and Tukey's multiple comparison post-test and *t*-tests; Fig. 5H). In the GA + Mo^{BM}-treated group a marked 2.8-fold increase in infiltrating inflammatory monocytes was detected (Fig. 5H).

The monocyte chemo-attractant protein 1 (MCP1/*CCL2*) is a key chemokine controlling recruitment of monocytes to inflamed CNS tissue (Izikson *et al.*, 2000; Deshmane *et al.*, 2009) and to the brain in murine Alzheimer's disease models (El Khoury *et al.*, 2007; Hickman and El Khoury, 2010). To evaluate whether the increased macrophage recruitment following immune-modulation treatment is mediated by elevated MCP1 in the brain, we analysed levels of soluble MCP1 in mouse brain homogenates by using a solid-phase sandwich ELISA kit (Fig. 5I). We found a significant elevation in brain MCP1 levels only in the combined GA + Mo^{BM} ADtg group; GA did not seem to elevate brain parenchymal MCP1 in these mice (Fig. 5I).

Local immune-modulation: elevated brain IL10 and MMP9

To analyse whether weekly injection of GA, Mo^{BM} adoptive transfer, or the combined GA + Mo^{BM} treatment affected cerebral IL10 expression, we first performed a qualitative immunohistochemical analysis of coronal brain sections (Fig. 6A–C; $n = 5$ mice per group). Brains were co-labelled with the markers Iba1 and CD45 and the anti-IL10 antibody. Representative fluorescence micrographs indicated low levels of IL10 expression in the brains of ADtg mice in the PBS control group (Fig. 6A), whereas a marked elevation in the levels of IL10, expressed both by microglia and monocytes, was especially apparent around amyloid-β plaques in the brains of mice in the GA and GA + Mo^{BM} groups (Fig. 6B and C). It is noteworthy that in the GA and GA + Mo^{BM} groups, we also found IL10 expressed by non-myelomonocytic $CD45^-/Iba1^-$ cells (Fig. 6C, arrow). A quantitative ELISA analysis of IL10 levels in brain samples validated a substantial increase in GA + Mo^{BM}-treated ADtg mice (2.2-fold increase in mean levels) compared to mice given PBS ($P < 0.05$; Fig. 6D). Compared to the PBS control group, the GA group had a 1.4-fold increase in cerebral IL10, which reached significance according to the unpaired Student *t*-test (Fig. 6D). This trend did not reach significance for the Mo^{BM} group.

We previously showed that a decreased amyloid-β burden in the brain was associated with local elevation of MMP9 (Koronyo-Hamaoui *et al.*, 2009), which is known to degrade amyloid-β. We therefore studied MMP9 expression by performing an immunohistochemical analysis of coronal brain sections from all mouse groups ($n = 5$ mice per group; Fig. 6E–H). We co-labelled the tissue with the markers Iba1, CD45, and MMP9. Representative fluorescence micrographs revealed basal MMP9 levels in the brains of PBS control ADtg mice (Fig. 6E), whereas increased amounts of MMP9 were frequently found in animals treated with GA, Mo^{BM}, or GA + Mo^{BM} (Fig. 6F–H). This increased MMP9 was accompanied by an increased number of infiltrating monocyte-derived macrophages ($Iba1^+/CD45^{high}$), which highly expressed MMP9 in the vicinity of the plaque. A quantitative ELISA analysis of MMP9 levels in brain samples indicated similar basal levels of cerebral MMP9 in brains from both PBS control ADtg mice and naïve wild-type controls (Fig. 6I). In contrast, brains of animals in the Mo^{BM} and GA + Mo^{BM} groups had significant increases of soluble MMP9 levels (1.6- and 1.7-fold increases, respectively; $P < 0.05$), compared to brains of animals in the PBS group. Although a trend of elevated MMP9 levels was observed in GA-treated mice, compared with PBS controls, this elevation did not reach statistical significance (Fig. 6I). No additive effect in MMP9 levels was observed for the combined treatment group. Previously published and current data indicate that following our immune-modulation treatment, there is a local molecular shift whose changes include a reduction in pro-inflammatory factors with increases in regulatory cytokines and amyloid-β-degrading enzyme levels.

Figure 6 Continued

finding was accompanied by an increase in infiltrating monocyte-derived macrophages ($Iba1^+/CD45^{high}$) highly expressing MMP-9 in the vicinity of the plaques. (**I**) Quantitative ELISA analysis of MMP9 levels in brain samples indicated similar basal levels of cerebral MMP9 in both PBS-injected ADtg mice and naïve wild-type controls. In contrast, the brains of ADtg mice treated with Mo^{BM} or GA + Mo^{BM} had a significant increase (1.6- and 1.7-fold, respectively) in soluble MMP9 levels, compared to the brains of control animals given PBS. Although the GA group displayed a trend toward elevated MMP9 levels, compared to the PBS control group, this did not reach statistical significance (NS). The intravariability in MMP9 values was very high in all treated groups and in the wild-type mouse group, compared to the relatively low variability in the PBS group. Group means and SEMs are shown. Fold increases in mean IL10 and MMP9 are indicated in red. $n = 4$–8 mice per each group. *$P < 0.05$.

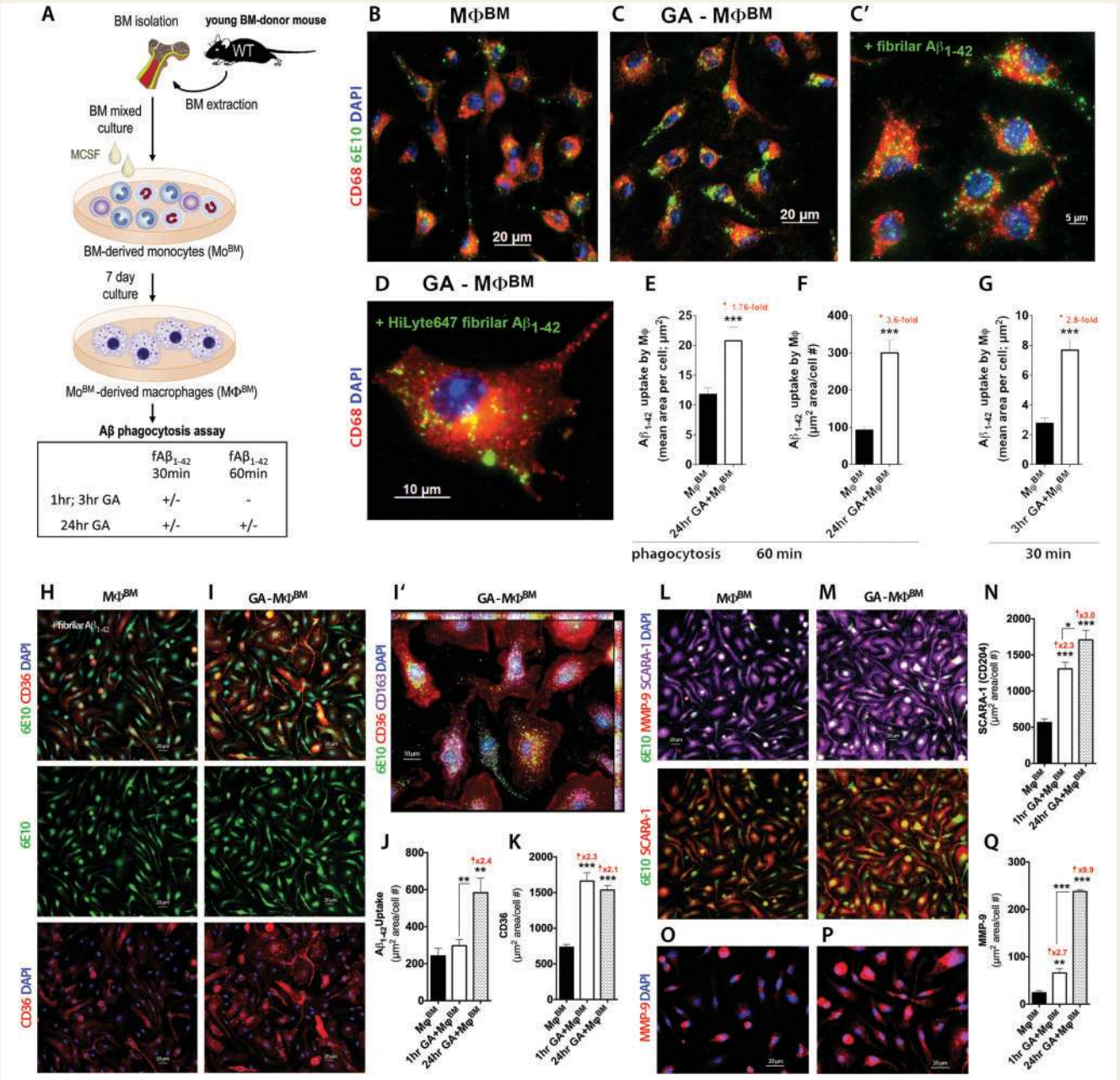

Figure 7 Enhanced fibrillar amyloid-β_{1-42} uptake by GA-treated macrophage *in vitro* is associated with increased expression of scavenger receptors and MMP9. (**A**) Illustration of experimental procedure: bone marrow was isolated from the long bones of young (8- to 10-week-old) wild-type mice and then cultured for 7 days in MCSF-enriched media providing differentiation into macrophages ($M\Phi^{BM}$). Upon differentiation, the cells were used in a set of experiments involving treatment with GA for different exposure times and stimulation with fibrillar amyloid-β_{1-42} ($fA\beta_{1-42}$), as indicated in the amyloid-β-phagocytosis assay design. (**B** and **C**) Representative fluorescence micrographs of $M\Phi^{BM}$ either (**B**) untreated or (**C**) pretreated with GA for 24 h (GA-$M\Phi^{BM}$) and both stimulated with fibrillar amyloid-β_{1-42} for 60 min. Cells were co-labelled with the phagocytic cell marker CD68 and anti-human amyloid-β mAb (6E10), and counterstained with DAPI. (**C'**) Higher-magnification image depicting the large extent of fibrillar amyloid-β_{1-42} uptake in GA-treated $M\Phi^{BM}$. (**D**) Image from a parallel *in vitro* experiment, using fluorescence-labelled (HiLyte Fluor 647) preformed fibrillar amyloid-β_{1-42}. (**E–G**) Quantitative immunocytochemistry of intracellular amyloid-β in GA-treated and untreated $M\Phi^{BM}$ primary cultures. (**E**) $M\Phi^{BM}$ were treated with GA for 24 h, exposed to fibrillar amyloid-β_{1-42} for 60 min, and intracellular amyloid-β staining was measured for each cell separately. Group means of individual cell fluorescent areas are indicated (n = 50 cells/group). (**F**) A parallel experiment, in which there was an analysis of overall amyloid-β-immunoreactive area divided by total cell count. Group means of n = 9–11 images of $M\Phi^{BM}$ cell cultures (average 170 cells/image) are presented. (**G**) An additional representative experiment, in which GA treatment was given for a shorter duration (3 h) and a shorter fibrillar amyloid-β_{1-42} phagocytosis assay (30 min). Group means of individual cell fluorescent areas are indicated (n = 70–100 cells/group). (**H–Q**) In the next set of experiments, $M\Phi^{BM}$ were pretreated for 1 or 24 h with GA and stimulated with fibrillar amyloid-β_{1-42} for 30 min. (**H** and **I**) Representative fluorescence micrographs of $M\Phi^{BM}$ either (**H**) untreated or (**I**) pretreated with 24 h GA and co-labelled with antibodies against CD36, an innate immunity scavenger receptor involved in amyloid-β binding and

(continued)

Enhanced fibrillar amyloid-$\beta_{1–42}$ uptake by GA-treated macrophages *in vitro* is associated with increased expression of scavenger receptors and MMP9

To investigate the possible effect of GA on the ability of macrophages to phagocytose amyloid-β, we performed a series of *in vitro* studies using macrophages in primary cultures. Bone marrow was isolated from young (8–10-week-old) wild-type mice and enriched in cultured monocyte-derived macrophages ($M\Phi^{BM}$) for 7 days. The $M\Phi^{BM}$ were then used in a set of experiments involving treatment with GA (30 µg/ml) for different exposure times and stimulation with 100 nM fibrillar amyloid-$\beta_{1–42}$, as presented in Fig. 7A, which illustrates the experimental procedure and amyloid-β phagocytosis assays. Representative fluorescence micrographs demonstrated that, as expected, $M\Phi^{BM}$ were capable of binding and internalizing preformed fibrillar amyloid-$\beta_{1–42}$ (Fig. 7B–D). Enhanced fibrillar amyloid-$\beta_{1–42}$ uptake was detected in GA-treated $M\Phi^{BM}$, as opposed to untreated $M\Phi^{BM}$, following a 24-h treatment with GA and a 60-min stimulation with fibrillar amyloid-$\beta_{1–42}$ (Fig. 7C versus 7B); fibrillar amyloid-$\beta_{1–42}$ uptake was assessed by intracellular staining of 6E10 in $CD68^+$ phagocytic myelomonocytic cells. A higher-magnification micrograph shows a large extent of fibrillar amyloid-$\beta_{1–42}$ uptake by GA-treated $M\Phi^{BM}$ (Fig. 7C′). This increased cellular uptake following GA treatment was also validated using fluorescently (HiLyte647)–labelled preformed fibrillar amyloid-$\beta_{1–42}$ (Fig. 7D). A series of quantitative immunocytochemical analyses of intracellular amyloid-β uptake by $M\Phi^{BM}$ after a 3- or 24-h treatment with GA and a 30- or 60-min exposure to fibrillar amyloid-$\beta_{1–42}$ indicated that, in all conditions, GA induced a substantial increase in the uptake of fibrillar amyloid-$\beta_{1–42}$ by $M\Phi^{BM}$ ($n = 9–12$ randomized areas; all $P < 0.0001$, Student *t*-test; Fig. 7E–G).

Amyloid-β clearance by $M\Phi^{BM}$ involves key mechanisms such as secretion of amyloid-β-degrading enzymes (such as MMP9) and expression of cell surface receptors that enhance amyloid-β binding and phagocytosis (for example, scavenger receptors such as CD36 (Hickman *et al.*, 2008; Yamanaka *et al.*, 2012) and SCARA1 [macrophage scavenger receptor 1 (*MSR1*), also known as CD204] (Frenkel *et al.*, 2013). To further characterize these GA-treated $M\Phi^{BM}$ in their response to fibrillar amyloid-$\beta_{1–42}$, additional *in vitro* experiments were performed during which $M\Phi^{BM}$ were either treated with GA for 1 or 24 h or untreated, and then stimulated with fibrillar amyloid-$\beta_{1–42}$ for 30 min (Fig. 7H–Q). Representative images show that increased fibrillar amyloid-$\beta_{1–42}$ uptake following GA treatment was coupled with increased expression of the class B scavenger receptor CD36 (Fig. 7I versus 7H). A high-magnification *Z*-stack image demonstrates substantial co-labelling of intracellular 6E10 and CD36 in GA-treated $M\Phi^{BM}$ and co-expression of another scavenger receptor, CD163, which has been implicated in Alzheimer's disease and the activation state of macrophages (Fig. 7I′) (Pey *et al.*, 2014). Quantitative analysis of intracellular 6E10 and CD36 in GA-treated $M\Phi^{BM}$ versus untreated (control) $M\Phi^{BM}$ validated that the significant increase in fibrillar amyloid-$\beta_{1–42}$ uptake was coupled with a significant 2.1- to 2.3-fold increase in CD36 expression ($P < 0.0001$, one-way ANOVA with Bonferroni's post-test; Fig. 7J and K). In addition, we analysed the expression levels of the innate immune scavenger receptor SCARA1 and the amyloid-β-degrading enzyme MMP9 in response to fibrillar amyloid-$\beta_{1–42}$ following GA treatment. A marked elevation in SCARA1 expression was observed in GA-treated $M\Phi^{BM}$, as opposed to untreated $M\Phi^{BM}$ (Fig. 7M versus 7L). A quantitative analysis of the SCARA1 immunoreactive area per cell confirmed significant 2.3- to 3-fold increases in SCARA1 expression with prolonged exposure to GA (1 h versus 24 h; $P < 0.0001$; Fig. 7N). Enlarged images demonstrate a substantial increase in MMP9 expression in GA-treated $M\Phi^{BM}$, as compared to untreated $M\Phi^{BM}$ (Fig. 7P versus 7O). A quantitative analysis indicated a remarkable 2.7- to 9.9-fold increase in cellular MMP9 expression by $M\Phi^{BM}$, especially following a 24-h treatment with GA ($P < 0.0001$; Fig. 7Q).

We next studied whether the observed phenotypic changes in the bone marrow-derived monocytes/macrophages that were used for adoptive transfer or primary $M\Phi^{BM}$ cultures were due to the positive isolation process with anti-CD115 antibody and magnetic beads in the MACS column (Supplementary Fig. 4). Initial flow cytometry analysis of $CD115^+$ mononuclear cells indicated that this isolation process substantially enriched this subpopulation of monocytes to ~95% (Supplementary Fig. 4A). A comparison analysis of bone marrow-derived cells before and after $CD115^+$ MACS column isolation

Figure 7 Continued

trafficking, human amyloid-β (6E10), and DAPI nuclei stain. (**I′**) Higher magnification *Z*-stack image depicting the large extent of fibrillar amyloid-$\beta_{1–42}$ uptake in GA-$M\Phi^{BM}$ associated with elevated CD36 and co-expression of another monocytic scavenger surface receptor, CD163. (**J–K**) Quantitative analysis of intracellular 6E10 (**J**) and CD36 (**K**) in the GA-$M\Phi^{BM}$ group versus the control $M\Phi^{BM}$ group. (**L–M**) Representative micrographs of $M\Phi^{BM}$ either untreated (**L**) or pretreated with 24 h with GA (**M**) and co-labelled with anti-CD204, an innate immune scavenger receptor known to facilitate amyloid-β phagocytosis (SCARA1), anti-MMP9, anti-human amyloid-β (6E10), and DAPI nuclei counterstaining. (**N**) Quantitative analysis of SCARA1 immunoreactive area per cell. (**O** and **P**) Enlarged images demonstrate MMP9 expression in the GA-$M\Phi^{BM}$ group (**P**) as compared to those from the $M\Phi^{BM}$ group (**O**). (**Q**) Quantitative analysis of cellular MMP9 in the GA-$M\Phi^{BM}$ group versus the control $M\Phi^{BM}$ group. Group means and SEM are shown, and fold increases in amyloid-$\beta_{1–42}$ uptake by macrophage are indicated in red. $^{**}P < 0.001$, $^{***}P < 0.0001$.

showed no significant alterations in cellular expression of SCARA1, MMP9 or CD36 within this CD115$^+$ monocyte subpopulation (Supplementary Fig. 4D–F). Moreover, these results were confirmed by quantitative immunocytochemistry analysis in primary cultures of bone marrow-derived macrophages before and after CD115$^+$ MACS column isolation (Supplementary Fig. 4G–I).

Discussion

This study demonstrates that weekly administration of the copolymer GA to a transgenic Alzheimer's disease animal model enhances natural recruitment of blood-borne monocytes to diseased brain parenchyma. Monthly enrichment of peripheral blood with the bone marrow-derived CD115$^+$ monocyte subset similarly increases cerebral recruitment of monocyte-derived macrophages. These two therapeutic protocols are highly beneficial to disease outcome, specifically due to their effects on retention of cognitive function, synaptic preservation, plaque removal, restriction of astrogliosis, and modulation of the immune molecular milieu. Combining the two treatment modalities results in more monocyte recruitment than either therapy alone; however, clinically, it provides no detected additive effect. Our study also indicates a molecular change in the brain, namely to elevated levels of the anti-inflammatory cytokine IL10 and the amyloid-β-degrading enzyme MMP9. Importantly, in the brains of all treated ADtg mice, infiltrating monocyte-derived macrophages became associated with parenchymal plaques and direct engulfment of amyloid-β. Our *in vitro* studies indicate that GA dramatically stimulated the capacity of MΦ^{BM} to phagocytose amyloid-$\beta_{1–42}$ fibrils, and this was coupled with similarly elevated co-expression of the scavenger receptors CD36 and SCARA1 as well as the amyloid-β-degrading enzyme MMP9.

Compared to brain resident microglia, macrophages appear highly efficient in phagocytosis of both parenchymal and perivascular amyloid-β deposition (Frautschy *et al.*, 1992; Simard *et al.*, 2006; Butovsky *et al.*, 2007; Fiala *et al.*, 2007; Majumdar *et al.*, 2008; Hawkes and McLaurin, 2009; Koronyo-Hamaoui *et al.*, 2009; Lebson *et al.*, 2010; Malm *et al.*, 2010, 2012; Lai and McLaurin, 2012; Michaud *et al.*, 2013; Bernstein *et al.*, 2014). Cerebral infiltration of murine blood-borne monocytes is specific to amyloidogenic amyloid-β accumulation (Malm *et al.*, 2010), and both human and murine myelomonocytes in primary cultures readily absorb amyloid fibrils (Paresce *et al.*, 1996; Webster *et al.*, 2000; Fiala *et al.*, 2005, 2007). In addition, *in vivo* studies in mice have shown that MCP1 and its receptor (CCR2) are critical for the migration and infiltration of Mo^{BM} to ADtg mouse brains (El Khoury *et al.*, 2007; Hickman and El Khoury, 2010; Lampron *et al.*, 2013; Naert and Rivest, 2013). Here, we demonstrate that in the combined (GA + Mo^{BM}) treatment group, the enhanced recruitment is explained, at least partially, by the significant increase in cerebral levels of MCP1.

The results of our study demonstrate that the capacity of bone marrow-derived macrophages to phagocytose amyloid-β can be substantially induced by GA stimulation (Fig. 7); phagocytosis of preformed fibrillar amyloid-$\beta_{1–42}$ was dramatically increased following both short-term (3-h) and long-term (24-h) exposures to GA. The enhanced capacity of GA-treated MΦ^{BM} to absorb fibrillar amyloid-$\beta_{1–42}$ was found to be tightly linked to elevated levels of the class A and B scavenger receptors SCARA1 and CD36, respectively, which are known to facilitate phagocytosis of amyloid-β and have been tightly implicated in Alzheimer's disease pathophysiology (Hickman *et al.*, 2008; Yamanaka *et al.*, 2012; Frenkel *et al.*, 2013; Pey *et al.*, 2014). Moreover, similar to our *in vivo* data, GA-treated MΦ^{BM} in culture exhibited increased expression of the amyloid-β-degrading enzyme MMP9, again a finding suggestive of an increased efficiency to clear toxic amyloid-β forms.

Because GA's chemical properties suggest that it acts in the periphery rather than crosses the blood–brain barrier, the observed increase in macrophage phagocytosis of amyloid-β in response to GA possibly indicates a direct effect of GA on monocytes/perivascular macrophages to trigger a peripheral sink effect for clearing toxic amyloid-β in the circulating blood and blood vessel walls. Future studies are required to determine possible effects of GA on the perivascular macrophage phenotype as well as on vascular amyloid-β clearance. The enhanced efficiency of GA-treated MΦ^{BM} to phagocytose fibrillar amyloid-$\beta_{1–42}$ raises two questions: (i) Can other altered myelin-derived antigens induce the same result in macrophages? and (ii) Does GA increase specific uptake of fibrillar amyloid-$\beta_{1–42}$ or instead global phagocytic activity? The latter question was partly addressed when Pul *et al.* (2012) observed that GA induced the general phagocytic capacity of macrophages.

The essential function of peripheral monocytes in murine models of Alzheimer's disease was demonstrated through selective ablation of these cells as well as by confining their cerebral migration via CCR2 inhibition or deficiency, which in turn accelerated disease progression (Butovsky *et al.*, 2007; El Khoury *et al.*, 2007; Naert and Rivest, 2013). Naert and Rivest (2013) showed that defective monocytopoiesis led to a reduction in CD115$^+$ (MCS-F receptor) monocytes in the blood of ADtg mice concurrent with the onset of cognitive decline, elevated amyloid-β levels, and reduced synaptic markers. An increased monocyte presence due to GA immunization or MCS-F injection (which increased bone marrow production of monocytes and their release into the blood), on the other hand, reduced amyloid-β levels and restored cognitive function (Butovsky *et al.*, 2007; Boissonneault *et al.*, 2009). These findings are valuable, although the studies involved techniques—such as whole-body irradiation and creation of chimeric mice, or local chemotherapy—that may have stimulated stronger than expected systemic immune responses in the brain.

The results of the present study indicate that blood enrichment with a subset of bone marrow-derived CD115$^+$

monocytes, in the absence of irradiation, genetic immune manipulation, or chemotherapy, results in a significant natural infiltration of monocytic cells into the cortical and hippocampal regions of murine models of Alzheimer's disease. Combining this approach with GA immunization seems to have a synergistic effect on this spontaneous cell recruitment into the hippocampi and cortices of ADtg mice. For this study, we used much younger bone marrow-donor mice than the recipient ADtg mice to increase the yield of the isolated CD115$^+$ monocytes. This raises a limitation in that we did not evaluate whether such effects could be also achieved with CD115$^+$ monocytes derived from aged mice. The blood-grafted GFP-labelled CD115$^+$ monocytes and endogenous infiltrating macrophage were tightly associated with both hippocampal and cortical plaques and direct engulfment of amyloid-β. This emphasizes the cells' natural ability to migrate to the diseased brain in response to aggregated amyloid-β and to accumulate inside and around plaques. This finding agrees with a previous report that showed infiltration of genetically modified peripheral CD11b$^+$ monocytes injected into the hearts of ADtg mice (Lebson *et al.*, 2010). In the present study, the PBS group had a relatively low ratio of infiltrating macrophage to amyloid-β plaque; in all treatment groups, however, the ratio was higher, as assessed by both the number of cells per plaque count and the immunoreactive area of cells per total plaque area, further indicating the cells' involvement in the clearance of plaque burden. These data were further confirmed by quantitative flow cytometry analysis of CD11b$^+$CD45^{high}Ly6C^{high} inflammatory monocytes in the brain. Notably, all treatment groups were associated with marked reductions in the amyloid-β plaque burden, soluble and insoluble amyloid-$\beta_{1\text{-}40}$ and amyloid-$\beta_{1\text{-}42}$, and astrogliosis, signifying the benefits in resisting Alzheimer's disease-associated neuropathology.

Infiltrating macrophages may clear amyloid-β from the brain not only through phagocytosis but also by secreting proteases that degrade amyloid-β. Macrophages co-cultured with amyloid-β-containing brain sections were shown to phagocytose amyloid-β and, moreover, to degrade amyloid-β by releasing MMP9 (Zhao *et al.*, 2009). Similar effects on restricting the cerebral amyloid-β plaque load were achieved by delivery of high-activity neprilysin, another amyloid-β-degrading enzyme, by grafted monocytes migrating to ADtg mouse brains (Lebson *et al.*, 2010). Substantial reductions in brain levels of soluble and insoluble amyloid-β were also demonstrated by targeting the overexpression of an amyloid-β-degrading enzyme—angiotensin-converting enzyme (ACE)—to myelomonocytic cells in ADtg mice (Bernstein *et al.*, 2014). In the present study we demonstrate, for the first time, the therapeutic effects of wild-type monocytes grafted into the peripheral blood of ADtg mice. Interestingly, adoptive transfer of this wild-type CD115$^+$ monocyte subset resulted in a local increase in MMP9 surrounding and within the plaque area, which was predominantly expressed by the infiltrating monocyte-derived macrophages. Grafting wild-type monocytes also led to a significant overall elevation of MMP9 levels in the brain, suggesting a mechanism of amyloid-β clearance via enhanced enzymatic degradation. GA further increased MMP9 expression in macrophage cultures.

GA has been shown to stimulate an anti-inflammatory response *in vivo*, reducing cerebral levels of pro-inflammatory TNF-α and elevating levels of IL10 and TGF-β1 by expanding helper T type 2/3 populations and shifting myelomonocytic profiles (Butovsky *et al.*, 2006; Aharoni *et al.*, 2007; Weber *et al.*, 2007). Following daily injections of GA to experimental autoimmune encephalomyelitis (EAE)–induced murine models, increased IL10 expression was observed in the brain (Arnon and Aharoni, 2004). Our study demonstrated that weekly injections of GA to ADtg mice resulted in a significant induction of regulatory IL10 levels in the brain. This is an important feature because IL10 targets innate immune and other glial cells in the brain and may aid in terminating detrimental neuroinflammation, which is a major pathological feature of Alzheimer's disease. Unlike the cerebral elevation of MMP9, which was prominently expressed by infiltrating monocytes in Mo^{BM}-grafted ADtg mouse groups, the elevation of IL10 was predominantly seen following GA immunization and not in animals that received Mo^{BM} grafts alone. The combined (GA + Mo^{BM}) treatment group showed a further fold increase in IL10 levels, which implies a synergistic effect. Similar to MMP9, IL10 expression was concentrated around amyloid-β plaques; however, following GA treatment IL10 was found to be highly expressed by several cell types, such as resident microglia, infiltrating macrophages, and local non-haematopoietic/myelomonocytic (Iba1$^-$/CD45$^-$) cells found also outside the cells surrounding the plaque. Additional studies should be performed to determine the nature and origin of these IL10-secreting cells following weekly GA immunization.

Finally, the ultimate goal of any Alzheimer's treatment is to preserve memory and learning abilities. As GA is an FDA-approved drug with high safety and tolerability records, and has been found to attenuate Alzheimer's disease-related cognitive decline and preserve the synaptic area associated with cognitive function, the drug holds great promise as a therapeutic intervention for Alzheimer's disease. Current and previously published data in animal models show that GA promotes neurogenesis and synaptic preservation, controls neuroinflammation, and targets and restricts several pathological features of Alzheimer's disease. In this study, symptomatic ADtg mice (10- to 13-months-old) were treated, and the observed benefits could therefore be proposed as disease modifying. It was striking to discover that blood enrichment with wild-type monocytes could preserve the hippocampal synaptic area and could reduce some aspects of behavioural deficits in this mouse model. Likewise, the combined (GA + Mo^{BM}) treatment group performed remarkably better in spatial learning and memory maze-based tests than PBS control animals. Some cognitive measurements in mice treated with GA (with or without Mo^{BM}) did not differ from

those in non-transgenic wild-type mice. Most encouraging was the overall association between the monocytes' natural migration to Alzheimer's disease-like brains and homing to plaque sites and the retention of learning and memory functions in this mouse model.

On the individual mouse level, we found that loss of synapses was associated with increased plaque area, and, moreover, with astrogliosis and cognitive deficits. Reduced astrogliosis, in particular, was strongly correlated with preservation of synapses and predicted improved memory retention scores. These observations provide the rationale for future testing of the feasibility of autologous monocyte administration, alone or in combination with a safe immune-modulation therapy, for therapeutic intervention in patients with Alzheimer's disease.

Acknowledgements

We thank Prof. Michal Schwartz for her critical and valuable advice on this manuscript. We thank Patricia Lin for assisting with the flow cytometry analysis. We also thank Drs Robert N. Pechnick and Catherine Farrokhi for helping with the behavioural studies, and Jo Ann M. Eliason, MA, ELS(D), for editing assistance. This paper is dedicated to the memory of Dr Salomon Moni Hamaoui and Lillian Jones Black, who both died from Alzheimer's disease.

Funding

This study was supported by the Coins for Alzheimer's Research Trust (C.A.R.T) Fund, the BrightFocus Foundation (former AHAF), The Marciano Family Foundation and The Saban Family Foundation and by the National Center for Advancing Translational Sciences through CTSI Grant UL1TR000124.

Supplementary material

Supplementary material is available at *Brain* online.

References

Aharoni R, Sonego H, Brenner O, Eilam R, Arnon R. The therapeutic effect of glatiramer acetate in a murine model of inflammatory bowel disease is mediated by anti-inflammatory T-cells. Immunol Lett 2007; 112: 110–9.

Akiyama H, Arai T, Kondo H, Tanno E, Haga C, Ikeda K. Cell mediators of inflammation in the Alzheimer disease brain. Alzheimer Dis Assoc Disord 2000a; 14 Suppl 1: S47–53.

Akiyama H, Barger S, Barnum S, Bradt B, Bauer J, Cole GM, et al. Inflammation and Alzheimer's disease. Neurobiol Aging 2000b; 21: 383–421.

Arnon R, Aharoni R. Mechanism of action of glatiramer acetate in multiple sclerosis and its potential for the development of new applications. Proc Natl Acad Sci USA 2004; 101 (Suppl 2): 14593–8.

Bakalash S, Pham M, Koronyo Y, Salumbides BC, Kramerov A, Seidenberg H, et al. Egr1 expression is induced following glatiramer acetate immunotherapy in rodent models of glaucoma and Alzheimer's disease. Invest Ophthalmol Vis Sci 2011; 52: 9033–46.

Bales KR, Du Y, Holtzman D, Cordell B, Paul SM. Neuroinflammation and Alzheimer's disease: critical roles for cytokine/Abeta-induced glial activation, NF-kappaB, and apolipoprotein E. Neurobiol Aging 2000; 21: 427–32.

Bates KA, Verdile G, Li QX, Ames D, Hudson P, Masters CL, et al. Clearance mechanisms of Alzheimer's amyloid-beta peptide: implications for therapeutic design and diagnostic tests. Mol Psychiatry 2009; 14: 469–86.

Bernstein KE, Koronyo Y, Salumbides BC, Sheyn J, Pelissier L, Lopes DH, et al. Angiotensin-converting enzyme overexpression in myelomonocytes prevents Alzheimer's-like cognitive decline. J Clin Invest 2014; 124: 1000–12.

Boissonneault V, Filali M, Lessard M, Relton J, Wong G, Rivest S. Powerful beneficial effects of macrophage colony-stimulating factor on beta-amyloid deposition and cognitive impairment in Alzheimer's disease. Brain 2009; 132: 1078–92.

Butovsky O, Koronyo-Hamaoui M, Kunis G, Ophir E, Landa G, Cohen H, et al. Glatiramer acetate fights against Alzheimer's disease by inducing dendritic-like microglia expressing insulin-like growth factor 1. Proc Natl Acad Sci USA 2006; 103: 11784–9.

Butovsky O, Kunis G, Koronyo-Hamaoui M, Schwartz M. Selective ablation of bone marrow-derived dendritic cells increases amyloid plaques in a mouse Alzheimer's disease model. Eur J Neurosci 2007; 26: 413–6.

Cairns NJ, Chadwick A, Luthert PJ, Lantos PL. Astrocytosis, beta A4-protein deposition and paired helical filament formation in Alzheimer's disease. J Neurol Sci 1992; 112: 68–75.

Deshmane SL, Kremlev S, Amini S, Sawaya BE. Monocyte chemoattractant protein-1 (MCP-1): an overview. J Interferon Cytokine Res 2009; 29: 313–26.

El Khoury J, Toft M, Hickman SE, Means TK, Terada K, Geula C, et al. Ccr2 deficiency impairs microglial accumulation and accelerates progression of Alzheimer-like disease. Nat Med 2007; 13: 432–8.

Fiala M, Cribbs DH, Rosenthal M, Bernard G. Phagocytosis of amyloid-beta and inflammation: two faces of innate immunity in Alzheimer's disease. J Alzheimers Dis 2007; 11: 457–63.

Fiala M, Lin J, Ringman J, Kermani-Arab V, Tsao G, Patel A, et al. Ineffective phagocytosis of amyloid-beta by macrophages of Alzheimer's disease patients. J Alzheimers Dis 2005; 7: 221–32; discussion 255–62.

Ford AL, Goodsall AL, Hickey WF, Sedgwick JD. Normal adult ramified microglia separated from other central nervous system macrophages by flow cytometric sorting. Phenotypic differences defined and direct ex vivo antigen presentation to myelin basic protein-reactive CD4+ T cells compared. J Immunol 1995; 154: 4309–21.

Frautschy SA, Cole GM, Baird A. Phagocytosis and deposition of vascular beta-amyloid in rat brains injected with Alzheimer beta-amyloid. Am J Pathol 1992; 140: 1389–99.

Frenkel D, Maron R, Burt DS, Weiner HL. Nasal vaccination with a proteosome-based adjuvant and glatiramer acetate clears beta-amyloid in a mouse model of Alzheimer disease. J Clin Invest 2005; 115: 2423–33.

Frenkel D, Wilkinson K, Zhao L, Hickman SE, Means TK, Puckett L, et al. Scara1 deficiency impairs clearance of soluble amyloid-beta by mononuclear phagocytes and accelerates Alzheimer's-like disease progression. Nat Commun 2013; 4: 2030.

Glezer I, Simard AR, Rivest S. Neuroprotective role of the innate immune system by microglia. Neuroscience 2007; 147: 867–83.

Hardy J, Selkoe DJ. The amyloid hypothesis of Alzheimer's disease: progress and problems on the road to therapeutics. Science 2002; 297: 353–6.

Hawkes CA, McLaurin J. Selective targeting of perivascular macrophages for clearance of beta-amyloid in cerebral amyloid angiopathy. Proc Natl Acad Sci USA 2009; 106: 1261–6.

Hickman SE, Allison EK, El Khoury J. Microglial dysfunction and defective beta-amyloid clearance pathways in aging Alzheimer's disease mice. J Neurosci 2008; 28: 8354–60.

Hickman SE, El Khoury J. Mechanisms of mononuclear phagocyte recruitment in Alzheimer's disease. CNS Neurol Disord Drug Targets 2010; 9: 168–73.

Izikson L, Klein RS, Charo IF, Weiner HL, Luster AD. Resistance to experimental autoimmune encephalomyelitis in mice lacking the CC chemokine receptor (CCR)2. J Exp Med 2000; 192: 1075–80.

Jankowsky JL, Fadale DJ, Anderson J, Xu GM, Gonzales V, Jenkins NA, et al. Mutant presenilins specifically elevate the levels of the 42 residue beta-amyloid peptide in vivo: evidence for augmentation of a 42-specific gamma secretase. Hum Mol Genet 2004; 13: 159–70.

Jankowsky JL, Slunt HH, Ratovitski T, Jenkins NA, Copeland NG, Borchelt DR. Co-expression of multiple transgenes in mouse CNS: a comparison of strategies. Biomol Eng 2001; 17: 157–65.

Juedes AE, Ruddle NH. Resident and infiltrating central nervous system APCs regulate the emergence and resolution of experimental autoimmune encephalomyelitis. J Immunol 2001; 166: 5168–75.

Kamphuis W, Middeldorp J, Kooijman L, Sluijs JA, Kooi EJ, Moeton M, et al. Glial fibrillary acidic protein isoform expression in plaque related astrogliosis in Alzheimer's disease. Neurobiol Aging 2014; 35: 492–510.

Kato S, Gondo T, Hoshii Y, Takahashi M, Yamada M, Ishihara T. Confocal observation of senile plaques in Alzheimer's disease: senile plaque morphology and relationship between senile plaques and astrocytes. Pathol Int 1998; 48: 332–40.

Koronyo-Hamaoui M, Ko MK, Koronyo Y, Azoulay D, Seksenyan A, Kunis G, et al. Attenuation of AD-like neuropathology by harnessing peripheral immune cells: local elevation of IL-10 and MMP-9. J Neurochem 2009; 111: 1409–24.

Koronyo-Hamaoui M, Koronyo Y, Ljubimov AV, Miller CA, Ko MK, Black KL, et al. Identification of amyloid plaques in retinas from Alzheimer's patients and noninvasive in vivo optical imaging of retinal plaques in a mouse model. Neuroimage 2011; 54: S204–17.

Lai AY, McLaurin J. Clearance of amyloid-beta peptides by microglia and macrophages: the issue of what, when and where. Future Neurol 2012; 7: 165–76.

Lampron A, Pimentel-Coelho PM, Rivest S. Migration of bone marrow-derived cells into the central nervous system in models of neurodegeneration. J Comp Neurol 2013; 521: 3863–76.

Lebson L, Nash K, Kamath S, Herber D, Carty N, Lee DC, et al. Trafficking CD11b-positive blood cells deliver therapeutic genes to the brain of amyloid-depositing transgenic mice. J Neurosci 2010; 30: 9651–8.

Liang H, Paxinos G, Watson C. Projections from the brain to the spinal cord in the mouse. Brain Struct Funct 2011; 215: 159–86.

Majumdar A, Chung H, Dolios G, Wang R, Asamoah N, Lobel P, et al. Degradation of fibrillar forms of Alzheimer's amyloid beta-peptide by macrophages. Neurobiol Aging 2008; 29: 707–15.

Malm T, Koistinaho M, Muona A, Magga J, Koistinaho J. The role and therapeutic potential of monocytic cells in Alzheimer's disease. Glia 2010; 58: 889–900.

Malm T, Magga J, Koistinaho J. Animal models of Alzheimer's disease: utilization of transgenic Alzheimer's disease models in studies of amyloid beta clearance. Curr Transl Geriatr Exp Gerontol Rep 2012; 1: 11–20.

Malm TM, Koistinaho M, Parepalo M, Vatanen T, Ooka A, Karlsson S, et al. Bone-marrow-derived cells contribute to the recruitment of microglial cells in response to beta-amyloid deposition in APP/PS1 double transgenic Alzheimer mice. Neurobiol Dis 2005; 18: 134–42.

Mawuenyega KG, Sigurdson W, Ovod V, Munsell L, Kasten T, Morris JC, et al. Decreased clearance of CNS beta-amyloid in Alzheimer's disease. Science 2010; 330: 1774.

McGeer PL, McGeer EG. Local neuroinflammation and the progression of Alzheimer's disease. J Neurovirol 2002; 8: 529–38.

Michaud JP, Bellavance MA, Prefontaine P, Rivest S. Real-time in vivo imaging reveals the ability of monocytes to clear vascular amyloid beta. Cell Rep 2013; 5: 646–53.

Naert G, Rivest S. A deficiency in CCR2+ monocytes: the hidden side of Alzheimer's disease. J Mol Cell Biol 2013; 5: 284–93.

Paresce DM, Ghosh RN, Maxfield FR. Microglial cells internalize aggregates of the Alzheimer's disease amyloid beta-protein via a scavenger receptor. Neuron 1996; 17: 553–65.

Pey P, Pearce RK, Kalaitzakis ME, Griffin WS, Gentleman SM. Phenotypic profile of alternative activation marker CD163 is different in Alzheimer's and Parkinson's disease. Acta Neuropathol Commun 2014; 2: 21.

Potter R, Patterson BW, Elbert DL, Ovod V, Kasten T, Sigurdson W, et al. Increased in vivo amyloid-beta42 production, exchange, and loss in presenilin mutation carriers. Sci Transl Med 2013; 5: 189ra77.

Prinz M, Priller J, Sisodia SS, Ransohoff RM. Heterogeneity of CNS myeloid cells and their roles in neurodegeneration. Nat Neurosci 2011; 14: 1227–35.

Renno T, Hahne M, MacDonald HR. Proliferation is a prerequisite for bacterial superantigen-induced T cell apoptosis in vivo. J Exp Med 1995; 181: 2283–7.

Richard KL, Filali M, Prefontaine P, Rivest S. Toll-like receptor 2 acts as a natural innate immune receptor to clear amyloid beta 1-42 and delay the cognitive decline in a mouse model of Alzheimer's disease. J Neurosci 2008; 28: 5784–93.

Rimoldi SF, de Marchi SF, Windecker S, Meier B, Allemann Y. Screening renal artery angiography in hypertensive patients undergoing coronary angiography and 6-month follow-up after ad hoc percutaneous revascularization. J Hypertens 2010; 28: 842–7.

Saido TC. Alzheimer's disease as proteolytic disorders: anabolism and catabolism of beta-amyloid. Neurobiol Aging 1998; 19: S69–75.

Selkoe DJ. Soluble oligomers of the amyloid beta-protein impair synaptic plasticity and behavior. Behav Brain Res 2008; 192: 106–13.

Shankar GM, Li S, Mehta TH, Garcia-Munoz A, Shepardson NE, Smith I, et al. Amyloid-beta protein dimers isolated directly from Alzheimer's brains impair synaptic plasticity and memory. Nat Med 2008; 14: 837–42.

Shechter R, London A, Varol C, Raposo C, Cusimano M, Yovel G, et al. Infiltrating blood-derived macrophages are vital cells playing an anti-inflammatory role in recovery from spinal cord injury in mice. PLoS Med 2009; 6: e1000113.

Simard AR, Soulet D, Gowing G, Julien JP, Rivest S. Bone marrow-derived microglia play a critical role in restricting senile plaque formation in Alzheimer's disease. Neuron 2006; 49: 489–502.

Takata K, Kitamura Y, Yanagisawa D, Morikawa S, Morita M, Inubushi T, et al. Microglial transplantation increases amyloid-beta clearance in Alzheimer model rats. FEBS Lett 2007; 581: 475–8.

Varol C, Landsman L, Fogg DK, Greenshtein L, Gildor B, Margalit R, et al. Monocytes give rise to mucosal, but not splenic, conventional dendritic cells. J Exp Med 2007; 204: 171–80.

Weber MS, Prod'homme T, Youssef S, Dunn SE, Rundle CD, Lee L, et al. Type II monocytes modulate T cell-mediated central nervous system autoimmune disease. Nat Med 2007; 13: 935–43.

Webster SD, Yang AJ, Margol L, Garzon-Rodriguez W, Glabe CG, Tenner AJ. Complement component C1q modulates the phagocytosis of Abeta by microglia. Exp Neurol 2000; 161: 127–38.

Wyss-Coray T. Inflammation in Alzheimer disease: driving force, bystander or beneficial response? Nat Med 2006; 12: 1005–15.

Wyss-Coray T, Lin C, Yan F, Yu GQ, Rohde M, McConlogue L, et al. TGF-beta1 promotes microglial amyloid-beta clearance and reduces plaque burden in transgenic mice. Nat Med 2001; 7: 612–8.

Wyss-Coray T, Mucke L. Inflammation in neurodegenerative disease–a double-edged sword. Neuron 2002; 35: 419–32.

Yamanaka M, Ishikawa T, Griep A, Axt D, Kummer MP, Heneka MT. PPARgamma/RXRalpha-induced and CD36-mediated microglial amyloid-beta phagocytosis results in cognitive improvement in amyloid precursor protein/presenilin 1 mice. J Neurosci 2012; 32: 17321–31.

Zhao L, Lin S, Bales KR, Gelfanova V, Koger D, Delong C, et al. Macrophage-mediated degradation of beta-amyloid via an apolipoprotein E isoform-dependent mechanism. J Neurosci 2009; 29: 3603–12.